



Reconstructing the geometry of central Anatolia during the late Cretaceous: Large-scale Cenozoic rotations and deformation between the Pontides and Taurides

Côme Lefebvre^{a,b,*}, Maud J.M. Meijers^{b,c}, Nuretdin Kaymakci^d, Ahmet Peynircioğlu^c, Cor G. Langereis^c, Douwe J.J. van Hinsbergen^e

^a Structural Geology and Tectonics Group, Department of Earth Sciences, Faculty of Geosciences, Utrecht University, Budapestlaan 4, 3584 CD Utrecht, The Netherlands

^b Géoazur, UMR 7329, Université de Nice Sophia Antipolis, Observatoire de la Côte d'Azur, Parc Valrose, 06108 Nice, France

^c Paleomagnetic Laboratory 'Fort Hoofddijk', Department of Earth Sciences, Faculty of Geosciences, Utrecht University, Budapestlaan 4, 3584 CD Utrecht, The Netherlands

^d Department of Geological Engineering, Middle East Technical University, 06531 Ankara, Turkey

^e Physics of Geological Processes, University of Oslo, Sem Sælands vei 24, NO-0316 Oslo, Norway

ARTICLE INFO

Article history:

Received 14 June 2012

Received in revised form

2 January 2013

Accepted 4 January 2013

Editor: T.M. Harrison

Keywords:

Central Anatolia
paleomagnetism
granitoids
rotation
collision

ABSTRACT

The Central Anatolian Crystalline Complex (CACC) exposes metamorphic, ophiolitic and igneous rocks that were formed and deformed during closure of the Neotethyan ocean. The CACC is located in central Turkey, between the Pontides in the north and the Taurides in the south, separated by major fault zones. Composite plutons intruded the meta-sedimentary and ophiolitic units between ~95 and 75 Ma, and form linear magmatic belts (~100 km long) along the western and northern margins of the CACC. Exhumation of the metamorphic and igneous complex was finalized by the Paleocene time. In this study, we paleomagnetically study fifteen plutons spanning the entire non-deformed upper Cretaceous granitoid belt to test whether the initial configuration of the CACC was modified by vertical axis rotations after its exhumation. Our results show three internally coherent domains with significantly different vertical-axis rotations: (1) in the north-east, the Akdağ–Yozgat block (AYB) records ~15° clockwise rotation, (2) in the north-west, the Kırşehir–Kırıkkale block (KKB) shows ~6–9° counterclockwise rotation and (3) in the south-west, the Ağaören–Avanos block (AAB) shows 28–35° counterclockwise rotation. We propose that these rotations were accommodated by two transpressional fault zones: in the south, the existing Savcılı Thrust Zone between the AYB and KKB and in the north, the newly introduced Delice–Kozaklı Fault Zone between the KKB and AAB. The restored configuration of the CACC suggests that the three blocks were largely aligned in a ~NNE orientation at an early stage of their history. Consequently, since the late Cretaceous the shape of the CACC was affected by large scale deformation, resulting in its modern triangular geometry. This deformation phase is best explained as a result of collision of the CACC with the Pontides.

© 2013 Elsevier B.V. All rights reserved.

1. Introduction

The Central Anatolian Crystalline Complex (CACC) is the largest metamorphic domain exposed in Turkey, and covers a triangular area of ~250 × 250 × 250 km (Fig. 1). Its tectonic history involves regional Barrovian metamorphism and wide-spread magmatism during the late Cretaceous (e.g. Erkan, 1976; Göncüoğlu, 1986; Whitney et al., 2003; Boztuğ and Jonckheere, 2007), followed by extension-driven exhumation of the crystalline rocks at the Earth's surface (Whitney and Dilek, 1997; Gautier

et al., 2002; Isik et al., 2008; Lefebvre et al., 2011, submitted for publication). However, the geodynamic context of its extension and exhumation remains poorly understood, mainly because soon after exhumation the CACC started colliding with the central Pontides in the Paleocene (Görür et al., 1984, 1998; Kaymakci et al., 2000, 2003a, 2003b, 2009; Meijers et al., 2010), leading to compression in central Anatolia throughout the Paleogene (Şengör and Yilmaz, 1981; Görür et al., 1984; Kaymakci et al., 2003b; Gülyüz et al., in press). Folding and thrusting affected basins surrounding (e.g. Çankırı, Tuzgölü, Sivas basins) and overlying (e.g. Kırıkkale, Çiçekdağ and Ayhan basins) the CACC (e.g. Görür et al., 1984, 1998; Poisson and Guezou, 1996; Köksal and Göncüoğlu, 1997; Dirik et al., 1999; Kaymakci et al., 2009; Advokaat, 2011; Gülyüz et al., in press) (Fig. 1b). The most prominent compressional feature in central Anatolia is the

* Corresponding author. Present address: Department of Earth Sciences, University of Minnesota, MN 55455, USA. Tel.: +1 612 624 8557.
E-mail address: lefebvre@umn.edu (C. Lefebvre).

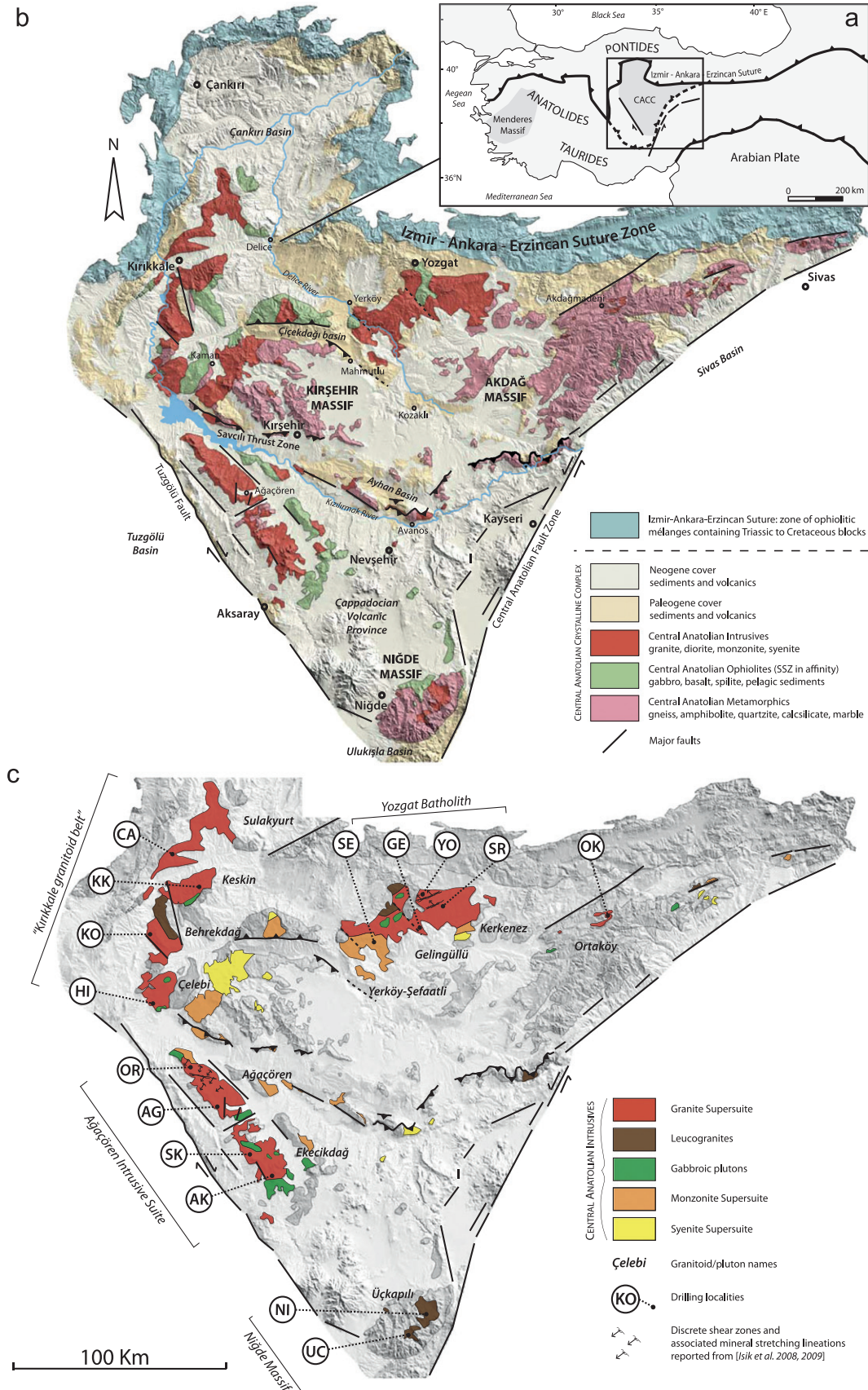


Fig. 1. (a) Simplified tectonic map of the Turkish orogenic system. The two gray areas indicate the location of the two largest metamorphic massifs in Turkey: the Menderes Massif and the Central Anatolian Crystalline Complex (CACC). (b) Simplified geological map of the CACC projected onto a Digital Elevation Model. (c) Composite map of the CACC showing (1) the distribution of the main central Anatolian magmatic supersuites (modified after Kadioğlu et al., 2006) and leucogranites (modified after Tatar et al., 1996); (2) the pattern of brittle faults affecting the plutons (after Erler and Göncüoğlu, 1996) and the discrete shear zones cutting across the Ağaçören and Kerkenez granitoids (after Isik et al., 2008; Isik, 2009); and (3) the locations and sampling codes of the fifteen paleomagnetic sampling localities, with the names of associated granitoids (after Akıman et al., 1993 for the western granitoids and after Erler and Göncüoğlu, 1996 for the Yozgat Batholith).

~150 km long EW-trending Savcılı Thrust Zone, which separates southern massifs (e.g. the Niğde Massif, Hırkadağ/İdişDağı Blocks and Ağaören Intrusive Suite) from the northern massifs (Kırşehir and Akdağ Massifs) (Oktay, 1982; Seymen, 2000; Genç and Yürür, 2010; Advokaat, 2011) (Fig. 1b).

The CACC exposes linear magmatic belts of late Cretaceous age along its southwestern, northwestern and northern margins defining a roughly NW-ward convex trend. Based on the tectonic evolution of the central Anatolian basins and scarce paleomagnetic data (Sanver and Ponat, 1981), Görür et al. (1984, 1998) proposed several tentative paleotectonic reconstructions. They speculated that the modern configuration of the CACC resulted from large-scale internal deformation and vertical-axis block rotations, transforming an originally elongated geometry into the present triangular shape, due to collision with the Pontides.

In this study, we paleomagnetically study the granitoids belts of the CACC to restore the late Cretaceous geometry of the CACC. We sampled 783 cores from fifteen localities that were evenly distributed over the CACC. We also compared our results with previous paleomagnetic studies carried out on upper Cretaceous–Miocene rocks within the CACC.

2. Geology of the CACC

As a segment of the Alpine-Himalayan orogenic belt, Turkey comprises a complex assemblage of continental and oceanic fragments (e.g. Ketin, 1966; Şengör and Yılmaz, 1981; Moix et al., 2008). In the north, the EW-trending Pontides is a Gondwana-derived fragment that contains Paleozoic metamorphic rocks overlain by a non-metamorphic Mesozoic cover (e.g. Şengör and Yılmaz, 1981). The Pontides are bounded by the Black Sea in the north and the Izmir–Ankara–Erzincan suture zone (IAESZ) in the south (Fig. 1a). The IAESZ marks the location of the former northern branch of the Neotethyan Ocean, comprising Triassic to Cretaceous oceanic remnants (radiolarites, carbonates, MORB-type basalts) and foreland basin clastics, deformed into a *mélange* (Brinkmann, 1972; Şengör and Yılmaz, 1981). To the south of the suture are exposed metamorphic rocks of the ‘Anatolides’, including the CACC, and non-metamorphic rocks of the ‘Taurides’, both overlain by upper Cretaceous ophiolites. Pan-African metamorphic basement and Paleozoic fauna demonstrate that the Anatolide–Tauride block(s) are derived from Gondwana (e.g. Okay, 1989; Kröner and Şengör, 1990).

The CACC is currently bounded by the IAESZ in the north, the dextral Tuz Gölü fault in the west and the sinistral Central Anatolian Fault Zone in the east, giving the CACC its triangular shape (Fig. 1b). The oldest rock units cropping out within the area consist of metamorphosed Paleozoic to Mesozoic clastic deposits and platform carbonates (Göncüoğlu et al., 1992; Kocak and Leake, 1994). During the Turonian–Santonian, these platform sediments underthrust below a supra-subduction type oceanic crust (referred as Central Anatolian Ophiolites (CAO) (Yaliniz and Göncüoğlu, 1998; Yaliniz et al., 2000) and underwent regional Barrovian metamorphism ranging from upper-amphibolite to greenschist facies, and therefore became the Central Anatolian Metamorphics (CAM) (Erkan, 1976; Seymen, 1981; Göncüoğlu et al., 1991) (Fig. 1). Metamorphism at peak conditions is estimated around 700–800 °C for 6–8 kbar with local re-heating at 2–4 kbar (Kocak and Leake, 1994; Whitney et al., 2001; Lefebvre et al., submitted for publication), associated with pervasive ductile deformation that developed penetrative foliation, isoclinal folds and shearing (Seymen, 1983; Tolluoğlu and Erkan, 1989; Lefebvre et al., submitted for publication). Following peak metamorphism, widespread plutons intruded both the CAM and CAO (Erdoğan et al., 1996; Erler and Göncüoğlu, 1996). This

magmatic event formed large, elongated plutons (~100 km long) that are mostly localized at, and follow the trend of the western and northern boundaries of the CACC (Akiman et al., 1993) (Fig. 1b). The composition of these intrusives covers a wide range, comprising both mafic and felsic intrusives, including gabbros, and granites, monzonites and syenites, respectively (Fig. 1c).

Various classification types have been applied and discussed in the literature in order to characterize the central Anatolian composite magmatics: (1) the alumina saturation index varying from peraluminous, metaluminous to peralkaline (e.g. Erler and Göncüoğlu, 1996; Aydın et al., 1998; Düzgören-Aydın et al., 2001), (2) the coexistence of S- (or C-), I- (or H-), and A-type granitoids illustrating the multiple magmatic sources (e.g. Aydın et al., 1998; Boztuğ, 2000; Düzgören-Aydın et al., 2001), (3) the presence of calc-alkaline, sub-alkaline and alkaline rock units (e.g. Ilbeyli et al., 2004; Ilbeyli, 2005; Kadioğlu et al., 2006), and (4) discrimination diagrams based on trace-elements indicating volcanic arc granite, syn-collisional granite, and within-plate granite fields for the granitoids, and mainly WPG field for the syenitoids (e.g. Akiman et al., 1993; Boztuğ, 2000; Ilbeyli, 2005; Kadioğlu et al., 2006).

Constraints on the age of emplacement of the plutons provided in the literature indicate that the magmatic pulse lasted from ~95 to 75 Ma (based on Rb/Sr whole rock, U/Pb on titanite and zircon and Pb/Pb evaporation on zircon methods) (Göncüoğlu, 1986; Whitney et al., 2003; Köksal et al., 2004, 2012; Boztuğ et al., 2007; Lefebvre et al., submitted for publication). However, the oldest crystallization ages are problematic, as they contradict field structural relations indicating that the central Anatolian magmatism postdates peak metamorphism in the CAM estimated at 91–84 Ma (Whitney et al., 2003; Whitney and Hamilton, 2004). Age constraints and crosscutting relationships provide the following spatial and temporal evolution: (1) the oldest granite supersuite occurs directly along the western and northern edges of the CACC forming an outer magmatic belt, (2) toward the center of CACC, the monzonite supersuite is intruding into the granites, and (3) the youngest syenite supersuite occurs as small plutonic bodies and is generally exposed in the inner part of the complex (Kadioğlu et al., 2006) (Fig. 1c).

Except for foliated leucogranites and some of the outer granitoids affected by discrete extensional ductile shear zones, the central Anatolian intrusives are generally ductily undeformed (Akiman et al., 1993; Boztuğ, 1998; Düzgören-Aydın et al., 2001; Isik et al., 2008; Isik, 2009) (Fig. 1c). Exhumation of the metamorphic/magmatic complex was associated with extensional detachments at the interface between the high-grade metamorphic rocks and essentially non-metamorphic remnants of the CAO, identified in the Niğde massif (Gautier et al., 2002), in the Kırşehir Massif near Kaman (Lefebvre et al., 2011), and in the Hırkadağ Block in the center of the CACC (Lefebvre et al., submitted for publication). The final unroofing stage of the central Anatolian crystalline rocks is constrained by apatite fission track data on granitoids, indicating a Paleocene age (~57–62 Ma) (Boztuğ and Jonckheere, 2007). Synchronously with this exhumation, basins of central Anatolia were filled by volcanic and sedimentary deposits (e.g. Görür et al., 1998; Dirik and Göncüoğlu, 1999; Kaymakci et al., 2009; Advokaat, 2011).

3. Paleomagnetic sampling, analysis, reliability and statistical treatment

3.1. Paleomagnetic sampling

In total, 783 cores were sampled at fifteen localities (each composed of five to eight sites) distributed within the upper Cretaceous igneous bodies. The drilling localities are concentrated within the outer magmatic belt to compare intrusive rocks from

the same magmatic period and with relatively similar composition (Fig. 1c). We aimed at sampling unfoliated and fresh outcrops of igneous rock away from brittle faulting.

All fifteen sampling localities are individual plutons that are geographically distributed within four main composite batholiths or magmatic suites (see Fig. 1c and Table 1), with compositions that range from granite, monzogranite to quartz monzonite (e.g. Akıman et al., 1993). The fifteen sampling localities are distributed as follows: (1) in the north-west of the CACC, a ~100 km long N–NNE trending magmatic belt (referred as “Kırıkkale granitoid belt” in Fig. 1c and Table 1) consists mainly of medium to coarse grained quartz monzonites and granites containing mafic enclaves (İlbeyli et al., 2004). Four sampling localities are located in individual granitoids from north to south: the CA locality from the Sulakyurt granitoid, KK from the Keskin granitoid, KO from the Behrekdağ granitoid, and HI from the Çelebi granitoid. Our samples consist mainly of hornblende–potassic feldspar granites. (2) In the west, a ~100 km long magmatic belt situated along the NW–SE trending Tuzgölü fault is known as the Ağaçören Intrusive Suite (AIS) (Kadioğlu and Güleç, 1996). The AIS is subdivided in the Ağaçören granitoid (Kadioğlu and Güleç, 1996) in the north and the Ekecikdağ granitoid in the south (Türeli, 1991). The granitoids mainly consist of coarse to porphyritic monzogranites, containing mafic enclaves. Four localities have been sampled from north to south: OR and AG from the Ağaçören granitoid and SK and AK from the Ekecikdağ granitoid. Our samples consist of hornblende–

biotite, biotite and hornblende–potassic feldspar granites. (3) In the north, the large Yozgat Batholith mainly consists of monzogranite and quartz monzonite, including eight granitoid subdivisions (Erler and Göncüoğlu, 1996). In our study, we sampled the western Yerköy–Şefaati granitoid (SE locality), the central Gelingüllü granitoid (GE locality) and the north-eastern Kerkenez granitoid (YO and SR localities, in the north and center of the pluton respectively). We completed the sampling with a locality further east of the Yozgat Batholith in the Ortaköy granitoid (OK locality) near the city of Akdağmadeni. Our samples consist of hornblende–biotite, hornblende–potassic feldspar and biotite granites. (4) Isolated in the southern Niğde Massif, the Üçkapılı granodiorite represents the southernmost pluton of the CACC. It consists of a two-mica monzogranite with a weakly developed ductile fabric (Göncüoğlu, 1986). The two sampling localities are NI and UC, and were collected from the central and north-eastern part of the granitoid, respectively. Our samples mainly consist of biotite–muscovite granites.

Age estimates of the sampled granitoids are based on existing radiometric data determined from the same or nearby magmatic pluton (see summary in Table 1). Note that the age of the magnetization is a cooling age, and is therefore younger than the crystallization age of the granitoids.

Ideally, sites within a locality were spaced ~50–100 m, a distance over which cooling may be sufficiently diachronous to average paleosecular variation. Per site the samples were drilled

Table 1
The main features of each sampling locality: their batholiths/magmatic suite, individual granitoids to which they belong, and the granite-type, the existing radiometric data with associated references and used dating methods.

Localities	Batholith/magmatic suite	Granitoid	Granite-type	Dating method	Age (Ma)	Samples; Reference
AG	Ağaçören intrusive suite	Ağaçören SE	HBG BMG	Rb/Sr (whole-rock) U–Pb (zircon)	110 ± 14 84.1 ± 1.0	Güleç (1994) Köksal et al. (2012)
AK	Ağaçören intrusive suite	Ekecikdağ SE	HBG		No data	
CA	Kırıkkale granitoid belt	Sulakyurt	HKG		No data	
GE	Yozgat Batholith	Gelingüllü	BG		No data	
HI	Kırıkkale granitoid belt	Çelebi	HKG		No data	
KK	Kırıkkale granitoid belt	Keskin	HKG	Pb–Pb (zircon) K–Ar (hbl)	77.0 ± 7.8 65–80*	Hasandede; Boztuğ et al. (2007) Hasandede; Boztuğ and Harlavan (2008)
KO	Kırıkkale granitoid belt	Behrekdağ	HKG	K–Ar (hbl) Pb–Pb (zircon) K–Ar (hbl+biot)	79.5 ± 1.7 92.4 ± 5.6 80–75*	İlbeyli et al. (2004) Konur; Boztuğ et al. (2007) Konur; Boztuğ and Harlavan (2008)
NI	Niğde Massif	Üçkapılı NE	BMG		No data	
OK	Akdağmadeni Suite	Ortaköy	HBG		No data	
OR	Ağaçören intrusive suite	Ağaçören NW	HKG		No data	
SE	Yozgat Batholith	Yerköy–Şefaati	HBG	K–Ar (hbl+biot)	80–68*	“ST”; Boztuğ and Harlavan (2008)
SK	Ağaçören intrusive suite	Ekecikdağ NW	BG	⁴⁰ Ar/ ³⁹ Ar (biot)	77.6 ± 0.3*	5; Kadioğlu et al. (2003)
SR	Yozgat Batholith	Kerkenez NW	HKG	⁴⁰ Ar/ ³⁹ Ar (hbl) ⁴⁰ Ar/ ³⁹ Ar (Ksp)	81.2 ± 0.5* 82.4 ± 0.3	03V-56; Isik et al. (2008) 03V-56; Isik et al. (2008)
UC	Niğde Massif	Üçkapılı SW	BMG	Rb/Sr (whole-rock) Rb/Sr (biot) K–Ar (biot) U–Pb SHRIMP (zircon) ⁴⁰ Ar/ ³⁹ Ar (biot) ⁴⁰ Ar/ ³⁹ Ar (biot) ⁴⁰ Ar/ ³⁹ Ar (Ksp) ⁴⁰ Ar/ ³⁹ Ar (Ksp) ⁴⁰ Ar/ ³⁹ Ar (biot) ⁴⁰ Ar/ ³⁹ Ar (musc)	95 ± 11 77.8 ± 1.2 78–75 92–85 76.2 ± 0.2 79.5 ± 1.2 70.3 ± 0.2 75.1 ± 1.0 76.0 ± 0.8	Göncüoğlu (1986) Göncüoğlu (1986) Göncüoğlu (1986) 98–16; Whitney et al. (2003) 95–59; Whitney et al. (2003) 98–17; Whitney et al. (2003) 98–17; Whitney et al. (2007) N49; Gautier et al. (2008) N67; Gautier et al. (2008)
YO	Yozgat Batholith	Kerkenez centre	HKG	⁴⁰ Ar/ ³⁹ Ar (biot)	80 ± 0.2	Sarhaçlı; Boztuğ et al. (2009)

BG=biotite granite, BMG=biotite–muscovite granite, HBG=hornblende–biotite granite, HKG=hornblende–potassic feldspar granite, and the existing radiometric data with associated references and used dating methods.

The ages marked by an asterisk are the ages used in Fig. 4.

within a range of several meters using a gasoline powered motor drill; details of all localities are presented in the [Supplementary Table](#). Sample orientations were measured with a magnetic compass and corrected for present-day declination (4.8 °E). Because we sampled plutonic bodies, we have no control on the paleohorizontal at the time of acquisition of the magnetization and therefore we are not able to apply a possible tilt correction. To check the validity of our data sets, we compared the paleolatitudes calculated from the data of our localities to those calculated from the Eurasian and African apparent polar wander (APW) path (Torsvik et al., 2008; see Fig. 4).

3.2. Paleomagnetic analysis

The 783 samples were cut into standard specimens, providing in most cases two or more specimens per core (referred to as A and B specimens, for the deeper and shallower part of the core respectively). A total of 1022 specimens was demagnetized. Thermal (TH) demagnetization of 80 specimens (14 steps from 20 to 580 °C) was carried out to verify the validity of alternating field (AF) demagnetization performed on 942 specimens (17 steps from 0 to 100 mT). AF demagnetization was carried out on the in-house developed robotized 2G DC SQUID magnetometer (noise level 10^{-12} A m²). Stepwise demagnetization of the natural remanent magnetization (NRM) is displayed in orthogonal vector diagrams (Fig. 2) (Zijderveld, 1967). Characteristic remanent magnetization (ChRM) directions were determined using principle component analysis (Kirschvink, 1980) on approximately five to seven successive temperature or AF steps in the majority of the specimens. Samples that yielded NRM components intermediate between two overlapping temperature or coercivity ranges were analyzed using the great-circle approach of McFadden and McElhinny (1988). This method determines the direction on the great circle that lies closest to the average direction of well-determined NRM directions. The great-circle approach was only used for four specimens from sites KK5, SK4 and SK6.

The magnetic carrier of the ChRM in the samples is magnetite, evidenced by maximum unblocking temperatures and fields around 580 °C and ~40–100 mT (see Fig. 2). Near-identical results for TH and AF demagnetization on specimens from the same sample were found (Fig. 2). The ChRM in several sites is removed in a high coercivity range (~80–100 mT or higher), which generally agrees with higher unblocking temperatures (~480–580 °C) in the specimens taken from the same samples (e.g. Fig. 2 o–p, aa–ab, and ad–ae). Demagnetization of the ChRM at low AF steps (~40–60 mT) generally coincides with lower unblocking temperatures (~250–400 °C; e.g. Fig. 2 l–m, af–ag and am–an).

Within a locality, and even within a site, specimens may carry both normal and reversed polarities. In most cases however, polarities were the same within one site. In several sites, samples were heavily affected by lightning (e.g. Fig. 4u and al), evidenced by their high intensities and single-component demagnetization diagrams. Most samples are affected by an overprint, which is likely a present-day field overprint (e.g. Fig. 4a, n, y, and z). Samples taken close to samples that were reset by a lightning strike often show a related overprint. Specimens affected by lightning as well as specimens with odd directions (e.g. N/up) were omitted from further analysis.

3.3. Reliability and statistical treatment

We calculated means from the ChRM directions and virtual geomagnetic pole (VGP) means using Fisher statistics (1953). The errors in declination (ΔD_x) and inclination (ΔI_x) were calculated separately from the A95 (the 95% cone of confidence of the VGPs) following Butler (1992). This approach is favored because it

describes the directional distributions more realistically: they become increasingly ellipsoidal (elongated) with lower latitudes (Creer et al., 1959; Tauxe and Kent, 2004; Deenen et al., 2011).

To test the reliability of our data and to identify potential vertical axis rotation and horizontal axis tilt differences within all sites and localities, we use the reliability criteria of Deenen et al. (2011) that depend on the number of samples (N). The Earth's magnetic field changes on short time scales of (tens) of thousands of years, the so-called paleosecular variation (PSV), implying that the magnetic field may vary in direction by $\pm 25^\circ$ or more (e.g. Jackson et al., 2000). With sufficient readings of the magnetic field over a sufficiently long time span (at least several tens of thousands of years), the geomagnetic field can be described as a geocentric axial dipole field (Merrill and McFadden, 2003). The criteria developed by Deenen et al. (2011) assess whether the statistical values of paleomagnetic datasets, expressed as the A95 cone of confidence of the VGPs, can be explained by paleosecular variation of the geomagnetic field alone. If that is the case, this dataset reliably represents geomagnetic field behavior, and no additional sources of scatter (such as differential vertical axis rotations or tilts within a sampled locality) have to be inferred within the averaged data set. These criteria are expressed as a confidence envelope between maximum and minimum values for A95 ($A95_{\max}$ and $A95_{\min}$), which are dependent on the number of samples (N). If a dataset provides an A95 smaller than $A95_{\min}$, PSV is underrepresented (e.g. the magnetic field is partially averaged within the samples, or samples were collected from rocks that do not cover sufficient time to average PSV). If A95 is larger than $A95_{\max}$, scatter of the dataset cannot be explained by PSV alone and additional sources of scatter have to be inferred, such as vertical axis rotations or tilt differences within the dataset.

These criteria are especially applicable when studying paleomagnetic directions in magmatic bodies, because the rate of cooling of a pluton at the scale of a single site is unknown. If the cooling rate is very high as in extrusive igneous rocks, site averages typically underrepresent PSV and display spot readings of the magnetic field (i.e. $A95$ values $< A95_{\min}$). In intrusive igneous rocks, however, cooling rates are likely to be much lower. To check whether the scatter within the individual sites can be explained by secular variation alone, we determined the $A95_{\min}$ and $A95_{\max}$ per site. In our case, practically all sites (82 out of 87) have $A95$ values that can be straightforwardly explained by PSV (see [Supplementary Table](#)). Because almost all sites represent PSV, we calculated mean ChRM direction per locality by averaging all individual ChRM directions. Thereafter a 45° cut-off on the locality-level was applied to remove outliers, and errors in declination (ΔD_x) and inclination (ΔI_x) were determined.

3.4. Anisotropy of magnetic susceptibility (AMS)

For nine localities, we performed measurements to determine the anisotropy of magnetic susceptibility (AMS) to assess the presence of a tectonic fabric, and whether formation of a fabric may have influenced the measured paleomagnetic direction. Even without tectonic deformation, most granites have a magmatic mineral fabric that results from alignment of phenocrysts during intrusion (magmatic foliation), which may be traced through AMS analysis (e.g. Denèle et al., 2011). We used Jelinek statistics (1981, 1984) for the calculation of the three tensor mean axes.

4. Results

4.1. Paleomagnetic results

Equal area projections of the ChRM directions of all localities and sites (represented by different symbols) are displayed in

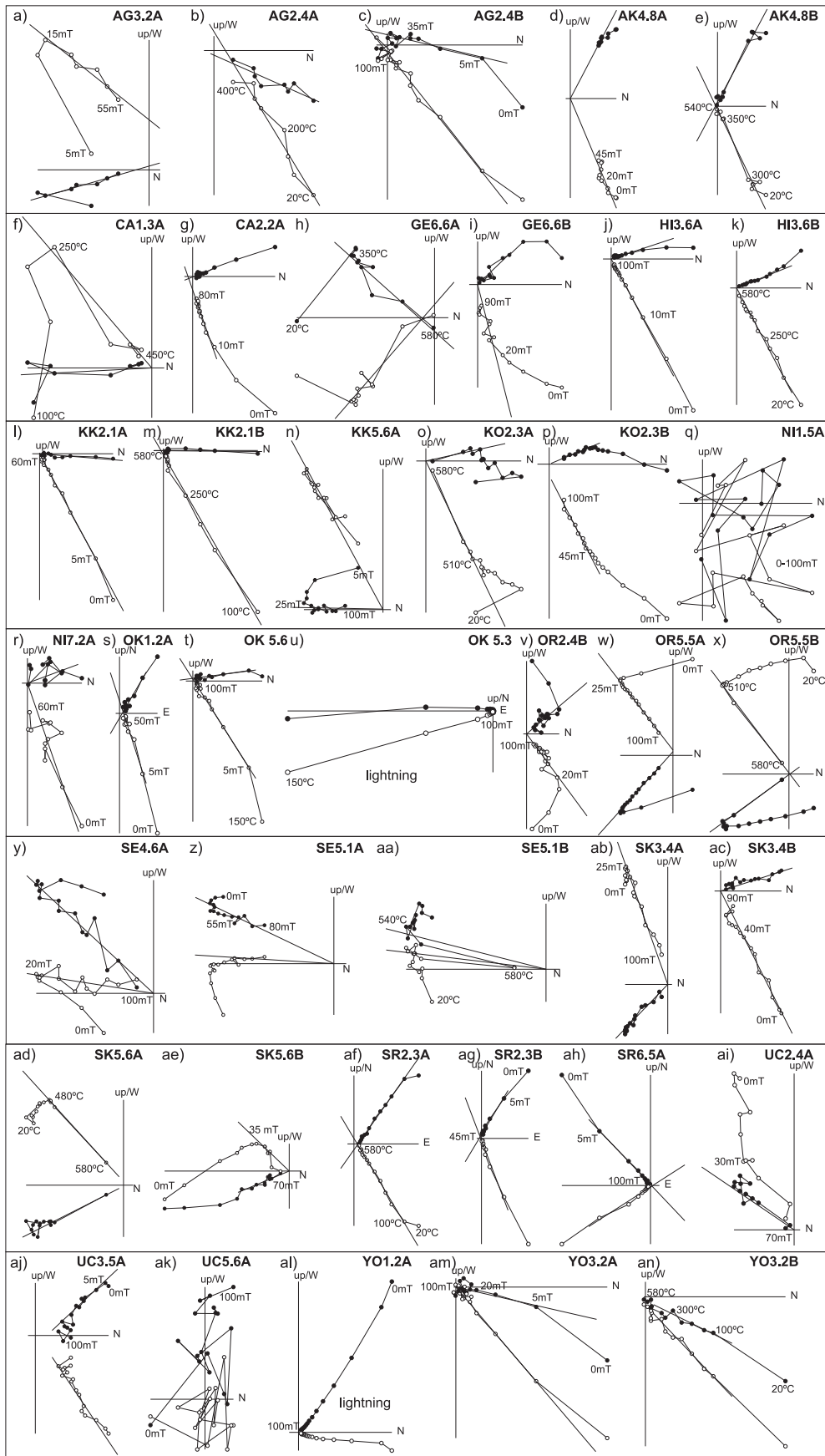


Fig. 2. Orthogonal vector diagrams (Zijderveld, 1967) showing representative demagnetization diagrams for all localities. Closed (open) circles indicate projection on the horizontal (vertical) plane. All diagrams are in a tilt corrected reference frame. For several samples, both alternating field (steps in milliTesla (mT)) and thermal (steps in °C) demagnetization diagrams are shown for two specimens from the same sample to show their similarity.

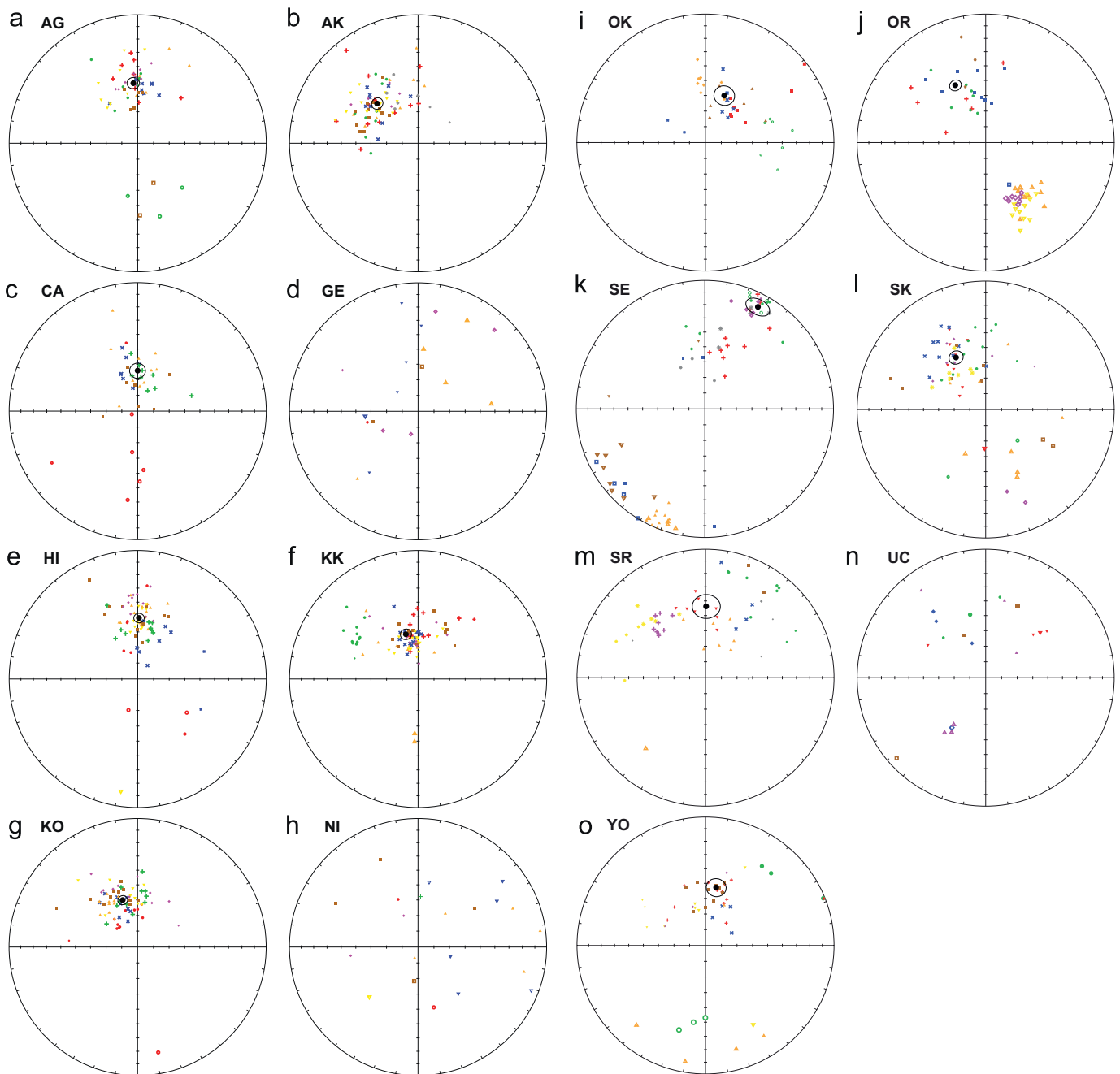


Fig. 3. Equal area projections of the ChRM directions for all localities and sites (all represented in different color/symbol) (Table 2a; Supplementary Table). Open (closed) symbols denote projection on upper (lower) hemisphere. Black symbols and circles represent respectively the mean ChRM direction per locality and their cone of confidence (α_{95}). Per locality, rejected data points (after application of fixed 45° cut-off) are displayed with small symbols. (For interpretation of the references to color in this figure legend, the reader is referred to the web version of this article.)

Fig. 3. Details per locality and per site can be found in the [Supplementary data and the Supplementary Table](#). Table 2a displays a synthesis of the calculated means and statistics per locality.

- For three localities (GE, NI and UC), the demagnetization of the NRM resulted in low quality data sets displaying very inconsistent and scattered ChRM directions (Fig. 3d, h, and n); therefore, we chose to not calculate mean ChRM directions for those localities and we do not consider them for further analysis.
- To check the reliability of the remaining data sets, we compared the A_{95} values on the locality level with the $A_{95_{\min}}$ and $A_{95_{\max}}$ of the Deenen et al. (2011) criteria. All localities yield A_{95} values that lie within the reliability envelope, except SR (Table 2a). Therefore, we regard all localities (except SR) as paleomagnetically ‘rigid’: i.e. there is no demonstrable internal rotation or tilt difference between the sites within a locality and each locality sufficiently averages PSV. In the case of locality SR, there are two sites showing counterclockwise and five sites showing (scattered) clockwise rotations, with an average declination of 0.0° . Because $A_{95} > A_{95_{\max}}$ statistically speaking there must be

Table 2(a)

All calculated means per locality and their statistical parameters.

Site	N_{sites}	N_{cores}	N_{demag}	N_a	N_{45}	D	I	λ	ΔD_x	ΔI_x	$K_{(vgp)}$	$A95_{(vgp)}$	$A95_{min}$	$A95_{max}$
AG	7	55	75	55	55	355.4	50.8	31.5	4.6	4.7	21.4	4.2	3.4	6.6
AK	8	60	84	76	74	314.4	53.0	33.6	5.3	4.6	15.1	4.4	3.0	5.4
CA	5	41	43	40	37	359.1	63.8	45.5	9.3	5.2	14.1	6.5	4.0	8.4
GE	7	51	53			No averages calculated								
HI	7	54	79	77	74	0.8	50.8	31.5	4.1	3.8	23.4	3.5	3.0	5.4
KK	7	50	93	89	86	344.3	60.5	41.5	5.9	3.8	13.1	4.4	2.9	5.0
KO	7	57	81	74	71	341.7	58.2	38.9	4.8	3.4	21.6	3.7	3.1	5.6
NI	7	46	46			No averages calculated								
OK	5	41	41	36	26	22.6	57.5	38.1	10.1	7.4	13.9	7.9	4.6	10.5
OR	7	51	75	59	59	331.9	48.3	29.3	4.5	4.5	23.1	3.9	3.3	6.3
SE	7	49	71	71	65	27.5	11.5	5.8	4.9	9.5	13.9	4.9	3.1	5.6
SK	7	55	79	64	60	329.8	51.4	32.1	6.0	5.5	14	5.1	3.3	6.2
SR	8	64	69	54	44								3.7	7.6
UC	7	57	57			No averages calculated								
YO	7	52	76	49	40	9.8	52.0	32.6	7.6	6.8	13.3	6.4	3.9	8.0
OK+YO (AYB)					66	14.5	54.4	34.9	6.2	5.1	12.9	5.1	3.2	5.9
CA+KK+KO+HI (KKB)					268	350.7	57.9	38.6	3.0	2.1	14.8	2.3	1.8	2.4
CA+KK+HI (KKB)					197	353.9	57.7	38.3	3.6	2.6	14	2.8	2.1	2.9
OR+SK+AK+AG (AAB)					248	331.6	51.9	32.5	3.1	2.8	12.7	2.6	1.9	2.5
OR+SK+AK (AAB)					193	324.8	51.3	32.0	3.2	3.0	14.8	2.7	2.1	3.0

N_s =number of sites per locality, N_{cores} =number of sampled cores, N_{demag} =number of demagnetized specimens, N_a =number of interpreted specimens, N_{45} =number of specimens included in the calculation for the mean CHRM direction after applying the 45° fixed cut-off (see [Supplementary data](#) for details per site), dec=declination, inc=inclination, λ =paleolatitude, ΔD_x (ΔI_x)=error in declination (inclination)calculated from the A95, $K_{(vgp)}$ =precision parameter determined from the mean virtual geomagnetic pole directions (VGPs), $A95_{(vgp)}$ =cone of confidence determined from the mean VGP direction, and $A95_{min}$ ($A95_{max}$)=minimum (maximum) value of the A95 for the given dataset based on [Deenen et al. \(2011\)](#). The strikethrough numbers of locality SR correspond to the value which does not pass the criteria $A95_{min} < A95 < A95_{max}$.

additional sources of scatter to PSV. We have no means of determining which sites are locally disturbed, and which are representative for the locality. Therefore, we discard locality SR from further analysis.

– Since we sampled plutonic rocks, we have no firm control on the paleohorizontal of the granitoids, and therefore a potential tilt correction cannot be applied. To check whether the calculated inclinations are within a ‘reasonable’ range, we translated the measured inclinations to paleolatitudes, and compared those with paleolatitudes of Eurasia and Africa in an age versus latitude plot ([Fig. 4](#)). We calculated the expected paleolatitudes of the Eurasian and African margins at the position of the city of Kırşehir ([Fig. 1](#)) with their error envelopes derived from the A95 values of the global Apparent Polar Wander Path (APWP) in Eurasian and African coordinates ([Torsvik et al., 2008](#)). To estimate the age of the sampled localities, we used the existing cooling ages as presented in [Table 1](#) (see $^{40}\text{Ar}/^{39}\text{Ar}$ and K–Ar ages marked by an asterisk). For the localities for which no radiometric ages are available, we used the age from the immediate neighboring plutons (AK \approx AG \approx OR \approx SK, CA \approx KK, HI \approx KO and OK \approx SR). The paleolatitudes corresponding to our localities plot within error on the Eurasian APW path, except for sites CA, KK (too high) and SE (too low) ([Fig. 4](#)). Also sites KO and OK give high paleolatitudes but are still within error of the expected values. During the late Cretaceous, the CACC was positioned between Eurasia and Africa, and therefore the paleolatitudes of sampled granitoids would be expected to plot between both paleolatitude curves. However, we must now conclude that the paleolatitude of the CACC was closer to the Eurasian curve than to the African one. This is in good agreement with the late Cretaceous–Paleocene initial collision of the CACC with the Pontides ([Kaymakci et al., 2003a](#); [Meijers et al., 2010](#)). The inclinations that we obtained for all localities are statistically indistinguishable from the Eurasian curve, with the exception of SE, CA, and KK. The few degrees offset from the Eurasian curve of the CA and KK localities are unlikely to result in large

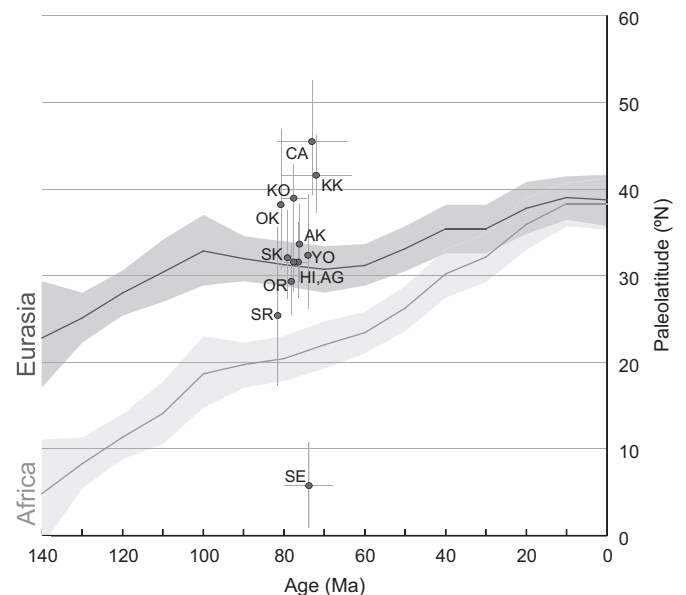


Fig. 4. Age versus latitude plot showing the curves for Africa and Eurasia calculated from the APW paths ([Torsvik et al., 2008](#)) with their $\Delta\lambda$ error (using the ΔI_x calculated from A95, shaded area). Calculated paleolatitudes from the accepted localities are plotted with their $\Delta\lambda$ error (calculated from the ΔI_x). The available isotopic ages used in the plot are the ones marked with an asterisk in [Table 1](#); the choice of the age for the undated granitoids is explained in [Section 4.1](#) (paleomagnetic results). Some ages were slightly shifted for the purpose of better display.

(more than several degrees) changes in rotation. Therefore, we decided to keep these localities for further analysis. Site SE however, yields a paleolatitude that differs $\sim 20^\circ$ from the Eurasian curve, probably as a result of tilting that may yield a significant rotation deviation. As a consequence, we omitted locality SE from further analysis.

In conclusion, according to the criteria above, ten localities were accepted for further analysis, while five localities (GE, SE and SR from the Yozgat Batholith, and NI and UC from the Niğde Massif) were rejected, as argued above.

4.2. AMS results

In Fig. 5, we present the results of AMS measurements for nine of the sampled localities. The AMS tensor shows oblate (HI, KK, OR, SE, SK) and prolate shapes (AG, AK, KO and SR). The orientation of the AMS tensor shows no obvious correlation with the mean ChRM direction (blue stars in Fig. 5) at a locality. It is interesting to note that the long axis orientations of the prolate ellipsoids of AG and AK and SR seem to correspond approximately with the strike of the mineral stretching

lineations reported from discrete ductile shear zones within the Ağaören and Yozgat Batholiths (Fig. 1c) (Isik et al., 2008; Isik, 2009). In general, however, there is no consistent or clear correspondence between AMS results, rotations and main tectonic directions, which would suggest that the magnetic fabric most likely represents magmatic foliations at the scale of individual plutons.

4.3. Paleomagnetic rotations and block definition

The accepted localities display a distinct pattern of rotation at the scale of the CACC (Fig. 6). On the basis of this pattern, we distinguished three domains with consistent and similar rotations that we defined as ‘blocks’ and for which we calculated mean

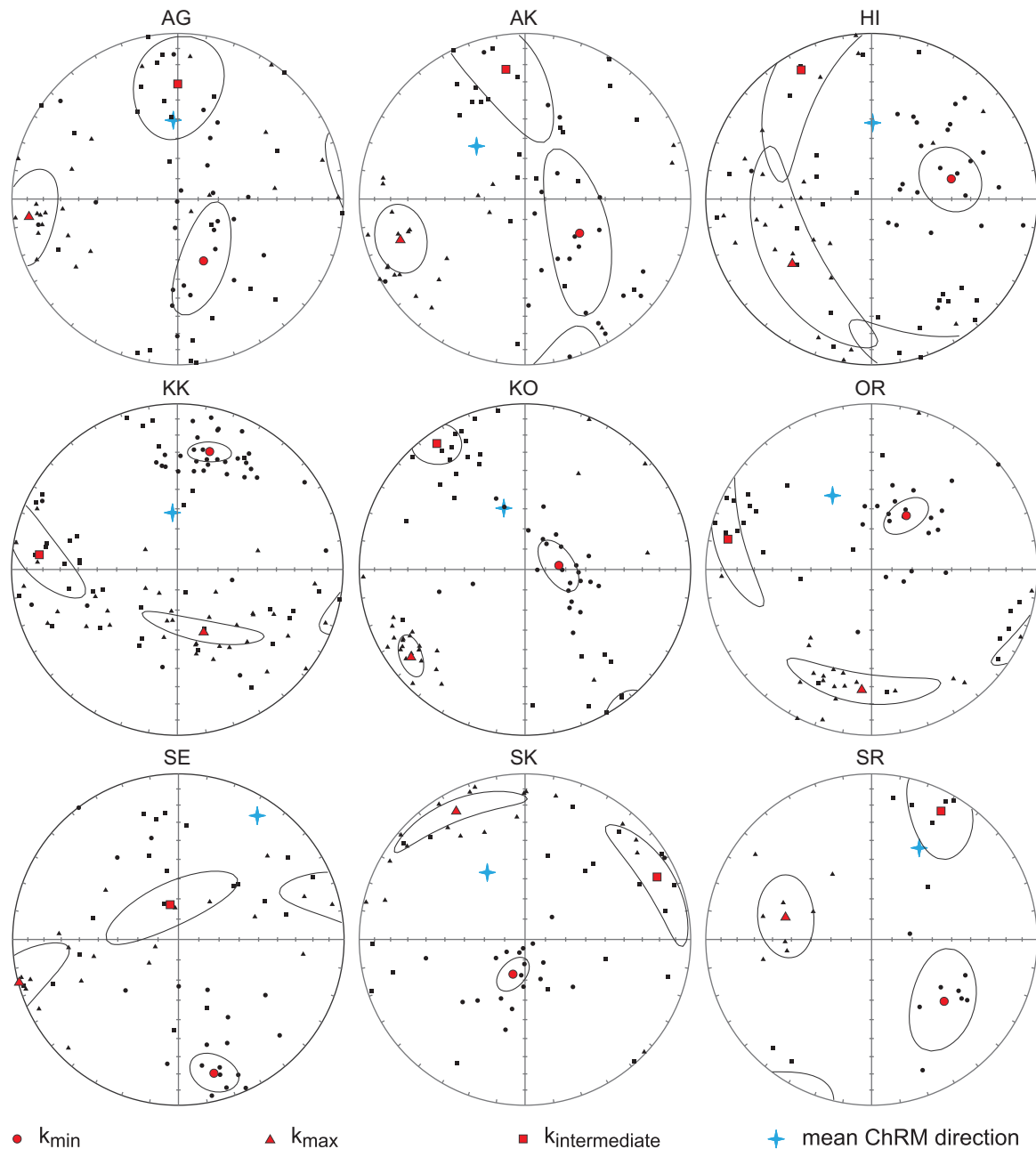


Fig. 5. Equal area projections of the anisotropy of magnetic susceptibility (AMS) of nine localities. Large red symbols indicate the mean of the tensor mean axes (k_{\min} =circles, k_{int} =squares, k_{\max} =triangles) and their 95% error ellipses (Jelinek, 1981). Blue stars indicate the ChRM direction of the locality mean. (For interpretation of the references to color in this figure legend, the reader is referred to the web version of this article.)

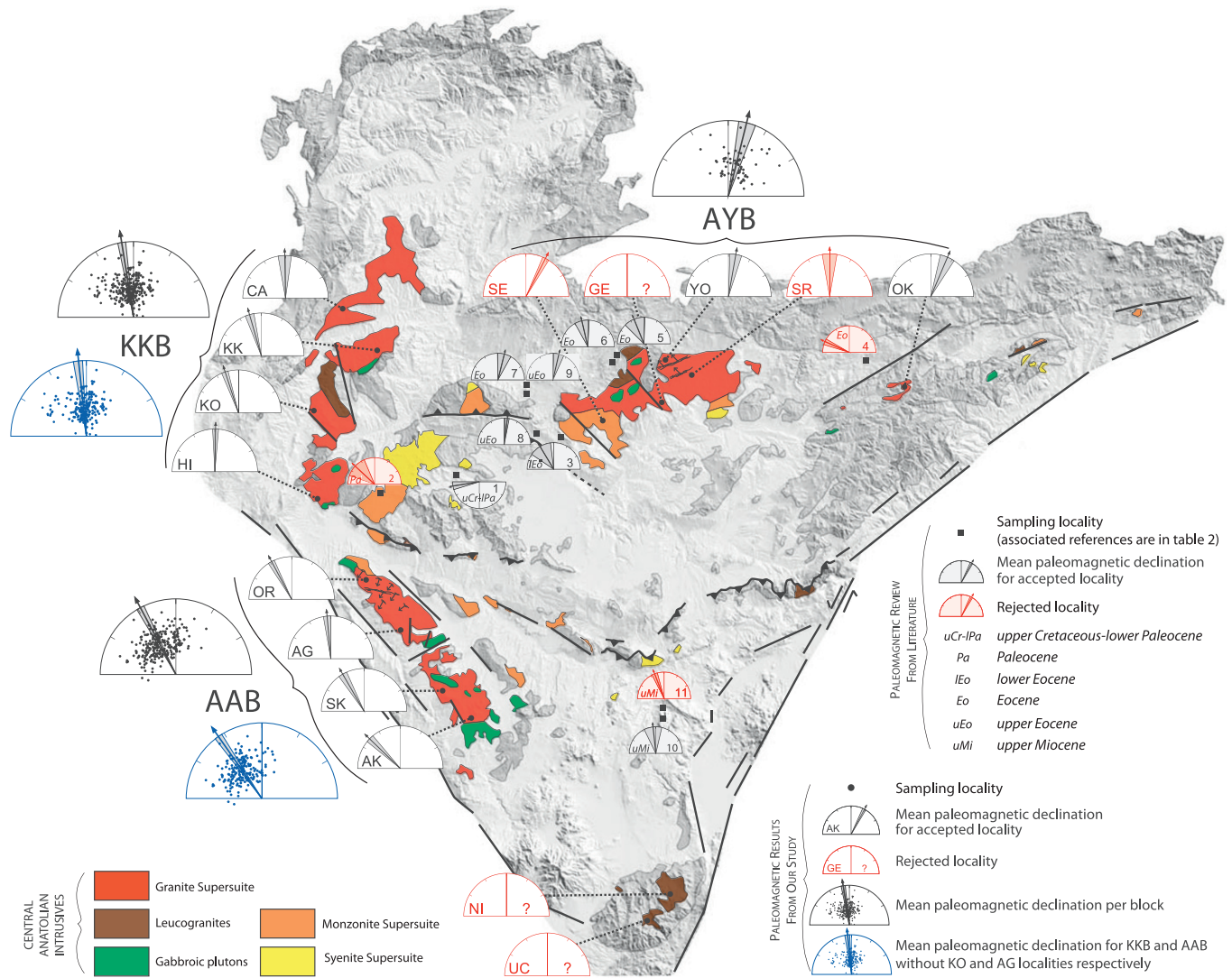


Fig. 6. Overview of all declinations and their error envelope (ΔD_x) per locality plotted on the regional geological map of the CACC. Rejected localities are indicated in red. The locality means per block (AAB, KKB and AYB) are indicated, as well as the locality means for KKB and AAB without KO and AG, respectively (in blue). Smaller declination plots represent the reviewed data from literature (Table 2b). (For interpretation of the references to color in this figure legend, the reader is referred to the web version of this article.)

rotations by averaging all individual ChRM directions (Fig. 6, Table 2a):

- (1) In the north-east, the two accepted localities (OK and YO) of the Akdağ–Yozgat block (AYB) (comprising the Akdağ metamorphic Massif and the Yozgat Batholith) show a $14.5^\circ \pm 6.2^\circ$ clockwise (CW) rotation. We note that the locality SE, even though rejected (see Section 4.1), also presents a comparable clockwise deviation tendency.
- (2) In the north-west, from the Kırşehir–Kırıkkale block (KKB) (comprising the Kırşehir metamorphic Massif and the “Kırıkkale granitoid belt”) the four localities (CA, KK, KO and HI) show a slight counterclockwise rotation (CCW): $9.3^\circ \pm 3.0^\circ$. Locality KO differs from the main tendency of the KKB presenting a significant CCW rotation; the mean rotation of the KKB block without locality KO would be $6.1^\circ \pm 3.6^\circ$ CCW.
- (3) In the south-west, the Ağaçören–Avanos block (AAB) (comprising the Ağaçören Intrusive Suite and the Hırkadağ/IdişDağı metamorphics) displays a significant counterclockwise rotation. The mean rotation of localities OR, AG, SK and AK is $28.4^\circ \pm 3.1^\circ$ CCW. Here, locality AG deviates from the main CCW tendency within the AAB; the mean rotation of the AAB block without locality AG would result in a larger CCW rotation of $35.2^\circ \pm 3.2^\circ$.

4.4. Comparison with previous paleomagnetic studies within the CACC: a short review

To integrate all paleomagnetic data from the region, we reviewed and compared our results with existing paleomagnetic data sets from the volcanic and sedimentary units covering the central Anatolian granitoids. Data from basins straddling the CACC were not taken into account, because these basins are likely affected by the major faults that define the boundaries of the CACC (e.g. the NAFZ and the Tuzgözü fault). For the purpose of this study, we reviewed available data from upper Cretaceous–Miocene rocks that cover and thus postdate the sampled granitoids (Table 2b). We calculated statistics on virtual geomagnetic poles (VGP’s) (K, A95) by averaging all site means per locality after applying a 45° cut-off on the sites (locality means could not be calculated from individual ChRM directions as was done for our own data sets because we did not have direct access to the original data sets). From the data collected by Piper et al. (2002) from the Miocene–Pleistocene volcanic fields of Cappadocia (Fig. 1), we calculated an average for Miocene lavas only. For Platzman et al. (1998) we obtained the A95 (and thus ΔD_x and ΔI_x) by using the Creer transformation (1962) on the α_{95} . Data sets from volcanic rocks with less than four sites per locality were

Table 2(b)
All reviewed paleomagnetic data from previous studies.

	Description	lat	lon	Age	Dec	Inc	λ	N	N ₄₅	k	ϕ_{95}	K	A95	ΔD_x	ΔI_x	Reference
1	Volcanics, Kaman	39.2	33.9	Upper Cret.–Pal. ^a	261.5	28.5	15.2	16	12	24.0	9.0	27.8	8.4	8.7	13.9	Sanver and Ponat (1981)
2	Volcanics and intrusives, Kaman	39.2	33.9	Paleocene	312.9	48.8	29.4	3	3	60.4	16.0	36.4	20.7	24.0	24.1	Kissel et al. (2003)
3	Volcanics, Kırşehir	39.5	34.5	Lower Eocene ^a	148.7	-54.6	35.2	10	8	11.3	17.2	8.6	20.1	24.8	20.1	Sanver and Ponat (1981)
4	Volcanics, Akdağmadeni	39.7	35.8	Eocene	293.9	43.5	25.4	3	3	573.0	5.2	429.4	6.0	6.6	7.7	Tatar et al. (1996)
5	Volcanics, Yozgat	39.8	34.7	Eocene	158.4	-46.5	27.8	5	5	17.9	18.6	14.6	20.7	23.6	25.1	Tatar et al. (1996)
6	Volcanics and sediments, Yozgat	39.8	34.4	Eocene	166.9	-12.5	6.3	7	7	8.0	22.8	15.5	15.8	15.9	30.6	Kissel et al. (2003)
7	Volcanics, Çiçekdağı	39.6	34.4	Eocene	194.3	-61.0	42.0	6	6	77.7	7.6	37.7	11.1	15.0	9.4	Gülyüz et al. (in press)
8	Sediments, Çiçekdağı	39.5	34.5	Upper Eocene	6.7	38.1	21.4	88	77	17.3	4.0	16.3	4.1	4.4	5.9	Gülyüz et al. (in press)
9	Sediments, Çiçekdağı	39.7	34.4	Upper Eocene	13.0	19.3	9.9	17	15	13.7	10.7	14.6	10.4	10.6	19.1	Gülyüz et al. (in press)
10	Ignimbrites, Cappadocia	38.6	34.8	Upper Miocene ^b	353.7	52.0	32.6	5	5	39.0	12.4	23.0	16.3	19.5	17.4	Piper et al. (2002)
11	Volcanics, Nevşehir	38.7	34.8	Upper Miocene ^c	159.0	-40.0	22.8	1	1	176.0	5.8	178.3	5.7	6.2	7.9	Platzman et al. (1998)

Description = the number we assigned to the study plus the rock type, plus the study location, lat (lon)=latitude (longitude) of the study location, Age = age of the sampled rocks, Dec (Inc)=declination (inclination) of the paleomagnetic results, λ = corresponding paleolatitude, N=number of sites (except for data sets 8 and 9 where the number of specimens is indicated), N₄₅=number of sites after applying the 45° fixed cut-off (except for data sets 8 and 9 where the number of specimens is indicated), k=estimate of the precision parameter determined from the ChRM directions, ϕ_{95} =cone of confidence determined from the ChRM directions, K=precision parameter determined from the mean virtual geomagnetic pole directions (VGPs), A95=cone of confidence determined from the mean VGP direction, and ΔD_x (ΔI_x)=error in declination (inclination) calculated from the A95. Studies that were accepted for further analysis are indicated in **bold**.

^a Ages poorly determined.

^b Mean was determined from Miocene data.

^c Site N6, consists of only one flow.

excluded from further analysis, because paleosecular variation was likely not averaged. This led to exclusion of the Paleocene data from Kissel et al. (2003), the Eocene data from Akdağmadeni from Tatar et al. (1996) and the Miocene data from Platzman et al. (1998). In Fig. 6, all reviewed data are presented together with the new obtained results from our study. The previous paleomagnetic studies are mainly concentrated in the northern and central parts of the CACC. Those studies were performed on sediments and volcanics that were deposited/emplaced on top of the outer granitoids of the KKB and AYB. Except for the study on the upper Cretaceous–Paleocene rocks from Sanver and Ponat (1981) (study 1 in Table 2b), the existing data suggest on average no vertical axis rotation pattern in the northern part of the CACC near Yozgat since the Eocene. The study on the volcanic fields of Cappadocia (Piper et al., 2002) shows in our analysis no significant post-Miocene vertical axis rotation.

5. Discussion

Paleomagnetic results from fifteen sampled localities belonging to the upper Cretaceous outer granitoids of the CACC show generally good results. Of the fifteen sampled localities, five localities were rejected because of inconsistent demagnetization behavior (resulting in very scattered ChRM directions), unsuccessful reliability test, and inconsistent paleolatitudes. Those five localities belong to the Niğde Massif (NI and UC) and the Yozgat Batholith (GE, SE and SR).

The Uçkapılı two-mica granite of the Niğde massif is considered as a late-kinematic intrusion as it locally contains a ductile fabric (Gautier et al., 2002; Whitney et al., 2003). We also observed this feature in the field and even though we aimed at sampling the least deformed bodies, it seems that the ductile fabric affected most of the granitoid and probably deteriorated the paleomagnetic signal. As a consequence, we have no independent rotational constraints from the southernmost part of the CACC.

In the Yozgat Batholith (localities GE, SE and SR), a dense network of deformation has affected the magmatic rocks (Erlor and Göncüoğlu, 1996; Isik et al., 2008). The presence of numerous brittle fault zones, like the NW–SE trending faults in the vicinity of the GE locality (see Fig. 1c), likely disrupted the structural coherence of the rock-unit and caused alteration and weathering that affected the magnetic signal. Since brittle faults are also present close to the sampling localities KO and AG (Fig. 1c), the same arguments may apply to explain why the results of these localities differ from the main tendency of the KKB and the AAB.

5.1. Restoration of the CACC

Based on the rotation pattern of the ten localities, we subdivided the CACC into three distinct blocks with consistent declinations: (1) the Akdağ–Yozgat block (AYB) in the northeast, that records $\sim 15^\circ$ CW rotation, (2) the Kırşehir–Kırıkkale block (KKB) in the northwest, that shows limited but significant ~ 6 – 9° CCW rotation and (3) the Ağaören–Avanos block (AAB) in the southwest, that shows ~ 28 – 35° CCW rotation. Note that these blocks also coincide with the magmatic suites or belts (the Yozgat Batholith, the “Kırıkkale granitoid belt” and the Ağaören Intrusive Suite respectively). As each of those ~ 100 km long batholiths records different and independent rotations, they can be described as paleomagnetically rigid structural entities during their post-emplacement tectonic evolution. In other words, they may be dissected by faults, but they are coherent in terms of vertical axis rotations. In Fig. 7, we illustrate various possible restorations for the central Anatolian granitoids and magmatic supersuites, based

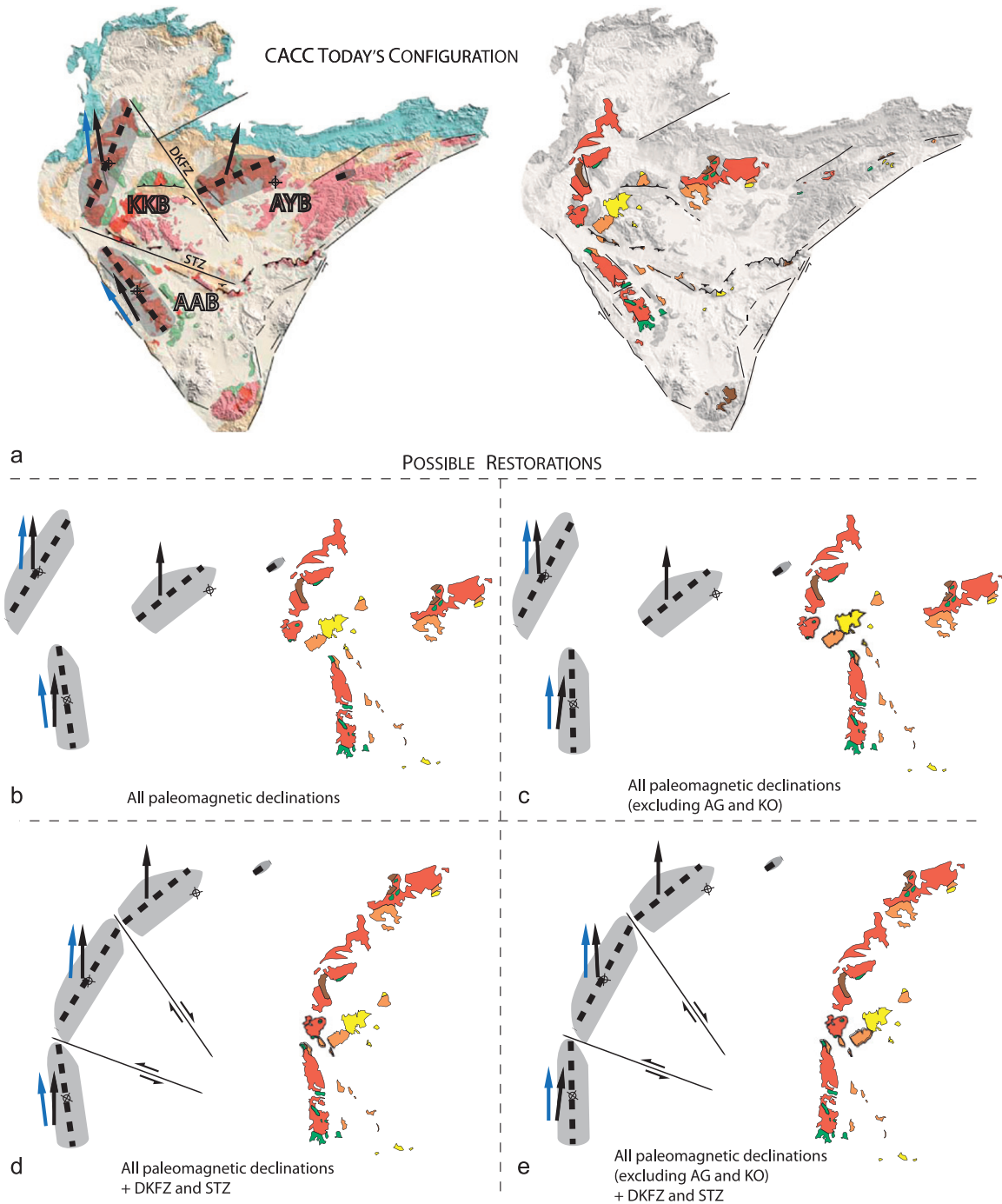


Fig. 7. Possible restoration scenarios of the late Cretaceous central Anatolian granitoids and magmatic Supersuites based on their rotations: (a) present-day configuration of the CACC. To the left, simplified geological map of the CACC, similar to Fig. 1. The gray domains represent the areas covered by the outer granitoids from the AAB, KKB and AYB; the dark dashed lines indicate the orientation of the long axis of the ellipsoid-like shaped batholiths. The black arrows indicate the mean declination per block. The blue arrows indicate the mean declination per block without taking localities AG and KO into account. In each block, the cross marks its center and the rotation pole we use for the restorations. The two black lines mark the possible trace of the dextral Kozaklı–Delice Fault Zone (DKFZ) and the sinistral Savcılı Thrust Zone (STZ). On the right, a background map of the CACC with the distribution of the main central Anatolian magmatic supersuites, similar to Fig. 1c. (b–e) Different restorations of the block rotations illustrated for the elongate-shaped granitoids (to the left), and for the magmatic supersuites (to the right): (b) for all mean declinations per block, with the absence of major strike-slip fault zones, (c) idem excluding AG and KO. (d) for all mean declinations per block, with the presence and motion along the two major strike-slip fault zones, and (e) idem excluding AG and KO. (For interpretation of the references to color in this figure legend, the reader is referred to the web version of this article.)

on the observed rotation patterns. We outlined the outer granitoids from the AAB, KKB and AYB and estimated the orientation of the long axis from the batholiths (Fig. 7a). We note that the orientations of their long axis coincide with the orientations of alignment of the highest peaks from the batholiths. Possible restorations of the CACC by back-rotation of the blocks are presented in Fig. 7b (all data) and c (excluding the deviating AG

and KO localities of AAB and KKB, respectively). Moreover, we remark that the edges of the newly defined blocks appear to be “truncated” (see Figs. 1b, c and 7a) and separated by narrow Eocene basins such as the Çiçekdağı and Ayhan basins (Fig. 1b). Within those basins, intense compressional deformation and significant horizontal shortening have been recently reported (Advokaat, 2011; Gülyüz et al., in press). Considering the

rotational pattern of the three blocks and the geology of the CACC, we propose the existence of two major transpressional strike-slip fault zones that have played a major role in accommodating the vertical axis rotations and associated horizontal displacements from a stage where all the granitoids were possibly linked and aligned together (Fig. 7d and e). It is also interesting to note that the two main fluvial systems of the region, i.e. the Kızılırmak river in the south and the Delice river in the north, seem to flow along the trace of the proposed fault zones, forming depressions of a few hundreds of meters below the average plateau elevation (Fig. 1b).

We define the two proposed fault zones as follows:

- (1) We postulate that the WNW–ESE trending limit between AAB and KKB coincides with the presence of the main tectonic structure recognized throughout the CACC: the Savcılı Thrust Zone (STZ) (Oktay, 1981; Seymen, 2000). This tectonic zone would correspond to a left-lateral transpressional zone which accommodated $\sim 30^\circ$ of counterclockwise rotation between the KKB and AAB (Fig. 7a). The sinistral lateral displacement estimated by the offset of the outer magmatic belt is approximately ~ 20 km. The relative amount of N–S shortening between the respective blocks, calculated from the length change of the granitoid belts, was estimated ~ 15 km in the west and increasing considerably toward the east (see Fig. 7a–d–e). This is consistent with the tectonic evolution of the Ayhan basin located in the eastern segment of the fault (Fig. 1b) where a pre-mid-Eocene volcano-sedimentary sequence was affected by north-vergent intense folding and thrusting (Genç and Yürür, 2010; Advokaat, 2011). Balanced cross-sections from this area revealed a minimum of 2 km N–S shortening, confirming intense compressional regime at the boundary of these blocks (Advokaat, 2011). The Savcılı Thrust Zone is described as a WNW-striking and SW-dipping fault carrying generally $\sim N10$ -oriented slickenlines (Caglayan and Isik, 2008), an orientation which corresponds well to the kinematic resulting from the relative motion between KKB and AAB.
- (2) We postulate that the NW–SE trending Delice–Kozaklı lineament represents the newly introduced right-lateral transpressional Delice–Kozaklı Fault Zone (DKFZ), which accommodated $\sim 20^\circ$ of clockwise rotation between the KKB and AYB (Fig. 7a). Along the DKFZ, the lateral dextral displacement estimated by the offset of the outer magmatic belt is as much as ~ 90 km. The relative amount of N–S shortening between the respective blocks was estimated as ~ 55 km (see Fig. 7a–d–e). Most of this shortening was accommodated by lateral dextral motion along the DKFZ.

Supporting the presence of the DKFZ, Genç and Yürür (2010) reported a NW–SE-oriented fold and thrust belt near the Mahmutlu village, north of the Savcılı Thrust Zone. In this area, Eocene limestones and younger detrital rocks are tilted in vertical positions and the related deformation was interpreted to take place within a contractional zone (Fig. 1b) (Genç and Yürür, 2010). This style of deformation causing the vertical position of sedimentary structures within a narrow corridor supports well our assumption of a transpressional fault zone. In addition, a network of NW–SE trending brittle faults has been reported in the western part of the Yozgat Batholith, adjacent to the DKFZ (Erler and Göncüoğlu, 1996). The orientation of these faults seems to coincide rather well with the proposed strike of the DKFZ (Fig. 1b). Interestingly, we also remark that the localities CA and KK (northern tip of the KKB) and SE (western border of the AYB) located on either of the DKFZ, presented abnormally high and low inclinations with respect to the age versus latitude curve of

Eurasia (Fig. 4). This may be linked to deformation associated with the right lateral displacement along the DKFZ. In Fig. 7d and e, we illustrate restorations including movement along the previously defined DKFZ and STZ. In their restored configurations, the three elongated magmatic belts appear in a similar, \sim NNE orientation and become approximately aligned into a single entity by motion along the DKFZ and STZ as described above. We infer that this configuration is probably the pre-rotational one, because the magmatic belts of granite, monzonite and syenite each align together. In the restored configuration, the granites are all concentrated on the western side of the NNE–SSW elongated structure, while monzonites and syenites occur consistently on the eastern side (Figs. 7d–e and 8).

5.2. Timing of rotations

The rotations recorded within the central Anatolian intrusives must postdate magmatic intrusion, and its cooling below the curie temperature of magnetite (the main carrier of the magnetization).

Most localities recorded both normal and reverse paleomagnetic field directions (see Fig. 3). The majority of the sites have a single polarity, but we also frequently observed normal and reversed polarities within a single site. At locality SK, we report the unique record of a change from reversed to normal polarity within the same core: the deeper part of the core (A) recorded a reversed polarity, whereas the shallow part (B) recorded a normal polarity (SK3.4A and B in Fig. 2ab and ac). This indicates that the Earth's magnetic field switched from reversed to normal polarity during cooling of the granite. At the exact location of locality SK, Kadioğlu et al. (2003) performed $^{40}\text{Ar}/^{39}\text{Ar}$ dating on biotites from the granitoid and found a cooling age (below $\sim 350^\circ\text{C}$) of 77.6 ± 0.3 Ma (Table 1). The recorded reversal may correspond to the reversed to normal polarity change at Chron C33 (Carnian) at ~ 79.6 Ma (Gradstein et al., 2004), which would imply that the magnetization was acquired earlier at a higher temperature, e.g. close to the Curie temperature of magnetite ($\sim 580^\circ\text{C}$).

The sparse existing paleomagnetic data from the upper Eocene and Miocene volcanic and sedimentary cover rocks on both sides of the DKFZ do not show any significant and regionally consistent rotation (Fig. 6). This may imply that the relative KKB/AYB rotation predates the deposition of the upper Eocene and younger cover rocks, but to confirm and refine the timing of block rotations in central Anatolia, extended sampling of Eocene and younger rock units is necessary.

However, we are unable to accurately constrain the timing of relative rotation between the KKB and AAB because there are no available paleomagnetic data of Paleogene age. Recently, the compressional deformation described in the Ayhan basin revealed a post-Lutetian shortening, which may have accommodated a considerable part of the KKB/AAB relative motion (Advokaat, 2011).

5.3. Regional implications

At a larger scale, we concur with Görür et al. (1984), that the internal deformation and vertical axis rotations within the CACC most likely relate to the collisional processes between the CACC and the Pontides. This scenario is also in good agreement with the established latest Cretaceous to earliest Paleocene inception of oroclinal bending of the central Pontides, as the CACC is located exactly south of the apex of the orocline (Kaymakci et al., 2003a; Meijers et al., 2010).

An important implication considering a NNE–SSW-oriented geometry for the CACC in the late Cretaceous is that its progressive northward collision with the central Pontides resulted in the break-up of the elongated structure into three distinctive pieces. Because the AYB presents the northernmost part of the CACC in the restored

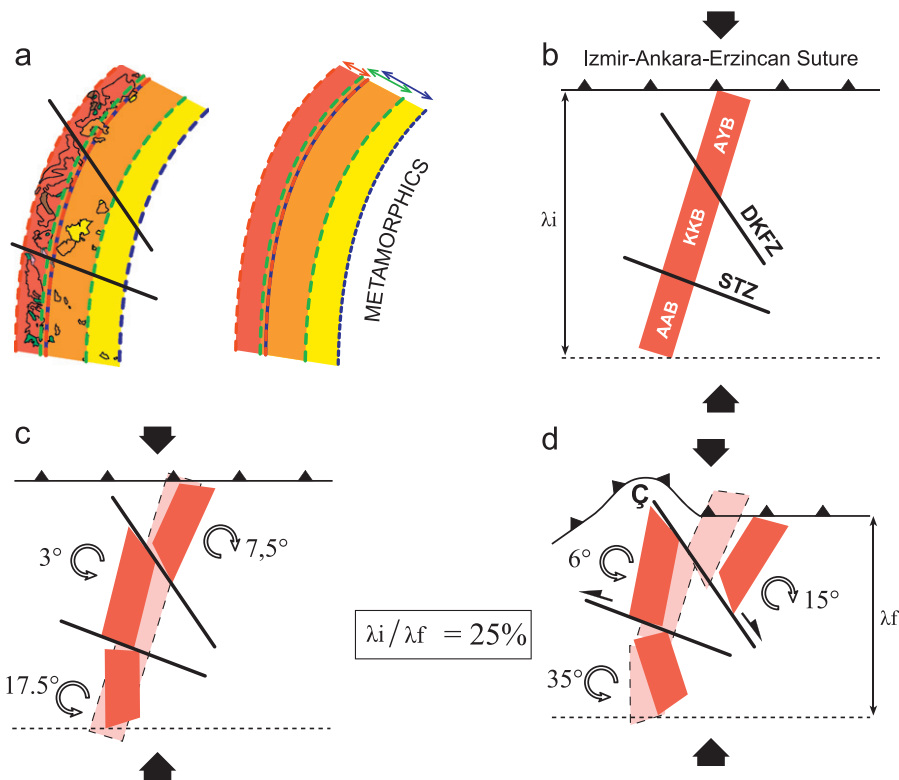


Fig. 8. Cartoons illustrating simplified scenario for the rotational evolution of the CACC. (a) Arrangement of supersuites of CACC after back rotation and translation along the DKFZ (~ 90 km) and STZ (~ 15 km). (b) Initial configuration of CACC. (c) Configuration at half-way rotation; note that the rotation of AYB and AAB are not necessarily contemporaneous (as illustrated). (d) Present configuration. Ç: Çankırı Basin.

configuration, it therefore would be the first to reach and collide with the accretionary prism of the IAESZ (Fig. 8b). In the scenario presented in Fig. 8, we propose that following frontal collision, the AYB underthrusts below the IAESZ, and resisted the ongoing convergence. As a consequence, the AYB likely rotated counter-clockwise, while the KKB extruded toward the north-west, “pushing away” the IAESZ and creating the Omega shape of the Çankırı basin (Fig. 8c and d). Together with the relative motion between the KKB and AAB, those deformations would imply a total of $\sim 25\%$ N–S shortening of the three initially connected blocks (Fig. 8d).

The granitoid belts may be regarded a rigid marker which can be used to estimate the amount of shortening taking place during collision with the Pontides. The comparison of the length of the modern and restored central Anatolian granitoid belt permits us to estimate a ~ 70 km N–S shortening (evolving from ~ 280 to 210 km). We note that the area south of the AIS until the Niğde massif (Fig. 1) was not taken into account for this calculation, because the paleomagnetic analysis on the Niğde leucogranites was unsuccessful.

Apart from the breaking up of the CACC, the restored configuration that proposes the late Cretaceous geometry to align the various magmatic supersuites presents a plausible solution (Fig. 7d and e). Indeed this would explain the distribution of the prominent magmatic belts and permit to propose a coherent model for the evolution of the CACC, as previous models almost always considered the triangular unrestored CACC as initial geometry. Therefore the new and crucial constraint that is provided by this study is that the tectonic setting responsible for the central Anatolian magmatism created a NNE–SSW-oriented plutonic belt of nearly 300×50 km at the time of cooling of the granitoids. The magmas were produced during ~ 20 Myr, and they evolved spatially and compositionally through time (from calc-alkaline silica-rich magmas in the west to alkaline silica-poor magmas in the east). Taking also the geochemistry into

consideration, which revealed that the granite and monzonite magmas derived from a modified and metasomatized mantle source (e.g. Ilbeyli, 2005; Kadioğlu et al., 2006), it is likely that the central Anatolian magmatic belt formed above a \sim NNE trending, E-dipping subduction zone. This new piece of information (i.e. the orientation of the proposed subduction) is rather surprising because at the scale of the Anatolian orogen, the main tectonic units and ancient oceanic tracts are generally structured in a W–E direction. Therefore, at the light of the interpretation of our new results here presented, we consider that two nearly orthogonal subduction systems (W–E trending below the Pontides in the north and \sim N–S trending below the CACC in the south) were synchronously active in Central Anatolia at the end of the Cretaceous.

6. Conclusions

Our paleomagnetic results from upper Cretaceous granitoids of central Anatolia show evidence for significant post-magmatic emplacement rotations. Three domains each presenting a consistent rotational pattern are distinguished:

(1) the Akdağ–Yozgat block (AYB) in the north-east recording $\sim 15^\circ$ CW rotation, (2) the Kırşehir–Kırıkkale block (KKB) in the north-west showing a slight CCW rotation (~ 6 – 9°) and (3) the Ağaçoören–Avanos block (AAB) in the south-west recording ~ 28 – 35° CCW rotation. We propose that these blocks were separated from each other by two major transpressional strike-slip fault zones: the sinistral Sıvılı Thrust Zone (STZ), and the dextral Delice–Kozaklı Fault Zone (DKFZ), which accommodated both rotation and translation of the blocks. Based on previous paleomagnetic data and the recently established latest Cretaceous to earliest Paleocene oroclinal bending scenario of the central Pontides, it seems likely that the rotation and internal deformation in the CACC occurred throughout most of the Paleocene–Eocene. The

most important outcome of this study is the restored original configuration of the CACC, showing that the three blocks were largely aligned in a \sim NNE orientation at an early stage of their history. This bears important implications concerning the tectonic reconstructions and evolutionary models of central Turkey within a major convergent setting, because the present geometry of the CACC does not correspond to its Cretaceous configuration.

Acknowledgments

The authors would like to dedicate this work to the memory of Tom Mullender, technician, electronics and gifted designer at the Paleomagnetic Laboratory Fort Hoofddijk in Utrecht, who greatly helped with the acquisition of the data presented in this article. Pınar Ertepinar and Murat Özkaptan are gratefully thanked for their precious help during the sampling process in the field. Merijn de Blok, Annique van der Boon, Lydian Boschman, Jort Koopmans, Matthijs Kroon, Roeland Nieboer, Katrien van Oversteeg, Joost Roholl and Anna van Yperen are thanked for their help analyzing samples. We appreciated technical support of Mark Dekkers. Reinoud Vissers is acknowledged for making the project possible. This work was financially supported by the Netherlands Research Centre for Integrated Solid Earth Sciences (ISES), the Netherlands Organisation for Scientific Research (NWO) and the DARIUS Programme.

Appendix A. Supplementary material

Supplementary data associated with this article can be found in the online version at <http://dx.doi.org/10.1016/j.epsl.2013.01.003>.

References

- Advokaat, E.L., 2011. Tectono-stratigraphic evolution of the Ayhan Basin, central Anatolia, Turkey: a late Cretaceous to early Eocene supra detachment basin that underwent post-Lutetian compression and tilting. M.Sc. Thesis. Utrecht University, Utrecht, The Netherlands.
- Akiman, O., Erler, A., Göncüoğlu, M.C., Güleç, N., Geven, A., Türeli, T.K., Kadioğlu, Y.K., 1993. Geochemical characteristics of granitoids along the western margin of the CACC and their tectonic implications. *Geol. J.* 28, 371–382.
- Aydın, S.N., Göncüoğlu, M.C., Erler, A., 1998. Latest Cretaceous magmatism in the CACC: review of field, petrographic and geochemical features. *Turkish J. Earth Sci.* 7, 259–268.
- Boztuğ, D., 1998. Post-collisional central Anatolian alkaline plutonism, Turkey. *Turkish J. Earth Sci.* 7, 145–165.
- Boztuğ, D., 2000. S-I-A-type intrusive associations: geodynamic significance of synchronism between metamorphism and magmatism in Central Anatolia, Turkey, vol. 173. Geological Society of London, Special Publications, pp. 441–458.
- Boztuğ, D., Jonckheere, R.C., 2007. Apatite fission track data from central Anatolian granitoids (Turkey): constraints on Neo-Tethyan closure. *Tectonics* 26 (3).
- Boztuğ, D., Tichomirowa, M., Bombach, K., 2007. ^{207}Pb – ^{206}Pb single-zircon evaporation ages of some granitoid rocks reveal continent–oceanic island arc collision during the Cretaceous geodynamic evolution of the Central Anatolia, Turkey. *J. Asian Earth Sci.* 31, 71–86.
- Boztuğ, D., Harlavan, Y., 2008. K–Ar ages of granitoids unravel the stages of Neo-Tethyan convergence in the eastern Pontides and central Anatolia, Turkey. *International Journal of Earth Sciences* 97, 585–599.
- Boztuğ, D., et al., 2009. Timing of post-obduction granitoids from intrusion through cooling to exhumation in central Anatolia, Turkey. *Tectonophysics* 473 (1–28), 223–233.
- Brinkmann, R., 1972. Mesozoic troughs and crustal structure in Anatolia. *Geol. Soc. Am. Bull.* 83 (3), 819–826.
- Butler, R.F., 1992. Paleomagnetism: magnetic domains to geologic terranes. Blackwell Scientific Publications, Boston.
- Caglayan, A., Isik, V., 2008. The Savcili Fault Zone, Central Turkey. *American Geophysical Union, Fall Meeting 2008*, Abstract #T51A-1866.
- Creer, K.M., Irving, E., Nairn, A.E.M., 1959. Paleomagnetism of the Great Whin Sill. *Geophys. J. R. Astron. Soc.* 2, 306–323.
- Creer, K.M., 1962. The dispersion of the geomagnetic field due to secular variation and its determination for remote times from paleomagnetic data. *J. Geophys. Res.* 67 (9), 3461–3476.
- Deenen, M.H.L., Langereis, C.G., van Hinsbergen, D.J.J., Biggin, A.J., 2011. Geomagnetic secular variation and the statistics of palaeomagnetic directions. *Geophys. J. Int.* 186, 509–520, <http://dx.doi.org/10.1111/j.1365-246X.2011.05050.x>.
- Denèle, Y., Lecomte, E., Jolivet, L., Lacombe, O., Labrousse, L., Huet, B., Le Pourhiet, L., 2011. Granite intrusion in a metamorphic core complex: the example of the Mykonos laccolith (Cyclades, Greece). *Tectonophysics* 501 (1–4), 52–70.
- Dirik, K., Göncüoğlu, M.C., Kozlu, H., 1999. Stratigraphy and pre-Miocene tectonic evolution of the southwestern part of the Sivas Basin, Central Anatolia, Turkey. *Geol. J.* 34, 303–319.
- Düzgören-Aydın, N.S., Maplas, J., Göncüoğlu, M.C., Erler, A., 2001. A review of the nature of magmatism in Central Anatolia during the Mesozoic post-collisional period. *Int. Geol. Rev.* 43, 695–710.
- Erdoğan, B., Akay, E., Uğur, M.S., 1996. Geology of the Yozgat Region and evolution of the collisional Çankırı Basin. *Int. Geol. Rev.* 38, 788–806.
- Erkan, E., 1976. Isogrades determined in the regional metamorphic area surrounding Kirşehir and their petrological interpretation (in Turkish with English summary). *Yerbilimleri* 2 (1), 23–54.
- Erler, A., Göncüoğlu, M.C., 1996. Geologic and tectonic setting of the Yozgat Batholith, Northern Central Anatolian Crystalline Complex, Turkey. *Int. Geol. Rev.* 38, 714–726.
- Fisher, D.A., 1953. Dispersion on a sphere. *Proc. R. Soc. London Ser. A* 217, 295–305.
- Gautier, P., Bozkurt, E., Hallot, E., Dirik, K., 2002. Dating the exhumation of a metamorphic dome: geological evidence for pre-Eocene unroofing of the Niğde Massif (Central Anatolia, Turkey). *Geol. Mag.* 139 (5), 559–576.
- Gautier, P., Bozkurt, E., Bosse, V., Hallot, E., Dirik, K., 2008. Coeval extensional shearing and lateral underflow during Late Cretaceous core complex development in the Niğde Massif, Central Anatolia, Turkey. *Tectonics* 27 (1).
- Genç, Y., Yürür, M.T., 2010. Coeval extension and compression in Late Mesozoic—recent thin-skinned extensional tectonics in central Anatolia, Turkey. *J. Struct. Geol.* 32 (5), 623–640.
- Göncüoğlu, M.C., 1986. Geochronological data from the southern part (Niğde area) of the Central Anatolian Massif. *Bull. Miner. Res. Explor. Inst. Turkish.* 105–106, 83–96.
- Göncüoğlu, M.C., Toprak, V., Kuşcu, I., Erler, A., Olgun, E., 1991. Orta Anadolu Masifinin orta bölümünün jeolojisi—bölüm 1: Güney kesim. *Turkish Petroleum Corporation (TPAO) Report no. 2909*, 140 pp (unpublished).
- Göncüoğlu, M.C., Erler, A., Toprak, V., Yalınız, K.M., Olgun, E., Rojay, B., 1992. Orta Anadolu Masifinin orta bölümünün jeolojisi—bölüm 2: Orta kesim. *Turkish Petroleum Corporation (TPAO) Report no. 3155* (unpublished), 76 pp (in Turkish).
- Görür, N., Oktay, F.Y., Seymen, I., Şengör, A.M.C., 1984. Palaeotectonic evolution of the Tuzgölü basin complex, Central Turkey: sedimentary record of a Neo-Tethyan closure, vol. 17. Geological Society of London, Special Publications pp. 467–482.
- Görür, N., Tüysüz, O., Şengör, A.M.C., 1998. Tectonic evolution of the central Anatolian basins. *Int. Geol. Rev.* 40 (9), 831–850.
- Gradstein, F.M., Ogg, J.G., Smith, A.G., Agterberg, F.P., Bleeker, W., Cooper, R.A., Davydov, V., Gibbard, P., Hinnov, L.A., House, M.R., Lourens, L., Luterbacher, H.P., McArthur, J., Melchin, M.J., Robb, L.J., Shergold, J., Villeneuve, M., Wardlaw, B.R., Ali, J., Brinkhuis, H., Hilgen, F.J., Hooker, J., Howarth, R.J., Knoll, A.H., Laskar, J., Monechi, S., Plumb, K.A., Powell, J., Raffi, I., Röhl, U., Sadler, P., Sanfilippo, A., Schmitz, B., Shackleton, N.J., Shields, G.A., Strauss, H., Van Dam, J., van Kolfschoten, T., Veizer, J., Wilson, D., 2004. A new geologic time scale, with special reference to Precambrian and Neogene. Cambridge University Press.
- Gülyüz, E., Kaymakci, N., Meijers, M.J.M., van Hinsbergen, D.J.J., Lefebvre, C., Vissers, R.L.M., Hendriks, B.W.H., Peynircioğlu, A., 2009. Late Eocene evolution of the Çiçekdağı basin (central Turkey): syn-sedimentary compression during microcontinent-continent collision in central Anatolia. *Tectonophysics*, in press.
- Güleç, N., 1994. Rb–Sr isotope data from the Ağaören granitoid (East of Tuz Gölü): geochronological and genetical implications. *Turkish Journal of Earth Sciences* 3, 39–43.
- İlbeyli, N., Pearce, J.A., Thirlwall, M.F., Mitchell, J.G., 2004. Petrogenesis of collision-related plutonics in Central Anatolia, Turkey. *Lithos* 72, 163–182.
- İlbeyli, N., 2005. Mineralogical-geochemical constraints on intrusives in central Anatolia, Turkey: tectono-magmatic evolution and characteristics of mantle source. *Geol. Mag.* 142 (2), 187–207.
- Isik, V., Lo, C.-H., Göncüoğlu, M.C., Demirel, S., 2008. $^{39}\text{Ar}/^{40}\text{Ar}$ ages from the Yozgat Batholith: preliminary data on the timing of late Cretaceous extension in the Central Anatolian Crystalline Complex, Turkey. *J. Geol.* 116 (5), 510–526.
- Isik, V., 2009. The ductile shear zone in granitoid of the Central Anatolian Crystalline Complex, Turkey: implications for the origins of the Tuzgölü basin during the Late Cretaceous extensional deformation. *J. Asian Earth Sci.* 34 (4), 507–521.
- Jackson, A., Jonkers, A.R.T., Walker, M.R., 2000. Four centuries of geomagnetic secular variation from historical records. *Philos. Trans. R. Soc. London, Ser. A: Math., Phys. Eng. Sci.* 358 (1768), 957–990.
- Jelinek, V., 1981. Characterization of the magnetic fabric of rocks. *Tectonophysics* 79 (3–4), T63–T67.
- Jelinek, V., 1984. On a mixed quadratic invariant of the magnetic-susceptibility tensor. *J. Geophys.—Z. Geophys.* 56 (1), 58–60.
- Kadioğlu, Y.K., Güleç, N., 1996. Mafic microgranular enclaves and interaction between felsic and mafic magmas in the Ağaören Intrusive Suite: evidence from petrographic features and mineral chemistry. *Int. Geol. Rev.* 38, 854–867.

- Kadıoğlu, Y.K., Dilek, Y., Güleç, N., Foland, K.A., 2003. Tectonomagmatic evolution of bimodal plutons in the central Anatolian crystalline complex, Turkey. *J. Geol.* 111 (6), 671–690.
- Kadıoğlu, Y.K., Dilek, Y., Foland, K.A., 2006. Slab break-off and syncollisional origin of the Late Cretaceous magmatism in the Central Anatolian crystalline complex, Turkey, vol. 409. Geological Society of America Special Papers pp. 381–415.
- Kaymakci, N., White, S.H., Van Dijk, P.M., 2000. Paleostress inversion in a multi-phase deformed area: kinematic and structural evolution of the Çankırı Basin (central Turkey), Part 1 - northern area. In: Bozkurt, E., Winchester, J.A., Piper, J.A.D. (Eds.), *Tectonics and Magmatism in Turkey and the Surrounding area* Geological Society London Special Publication, 173; pp. 445–473.
- Kaymakci, N., Duermeijer, C.E., Langereis, C., White, S.H., Van Dijk, P.M., 2003a. Palaeomagnetic evolution of the Çankırı Basin (central Anatolia, Turkey): implications for oroclinal bending due to indentation. *Geol. Mag.* 140 (3), 343–355.
- Kaymakci, N., White, S.H., Vandijk, P.M., 2003b. Kinematic and structural development of the Çankırı Basin (central Anatolia, Turkey): a paleostress inversion study. *Tectonophysics* 364 (1–2), 85–113.
- Kaymakci, N., Özçelik, Y., White, S.H., Van Dijk, P.M., 2009. Tectono-stratigraphy of the Çankırı Basin: late Cretaceous to early Miocene evolution of the Neotethyan Suture Zone in Turkey, vol. 311. Geological Society, Special Publications, London, pp. 67–106.
- Ketin, I., 1966. Tectonic units of Anatolia (Asia Minor). *Bull. Miner. Res. Explor.* 66, 23–34.
- Kirschvink, J.L., 1980. The least-square line and plane and the analysis of paleomagnetic data. *Geophys. J. R. Astron. Soc.* 62, 699–718.
- Kissel, C., Laj, C., Poisson, A., Görür, N., 2003. Paleomagnetic reconstruction of the Cenozoic evolution of the Eastern Mediterranean. *Tectonophysics* 362, 199–217.
- Kocak, K., Leake, B.E., 1994. The petrology of the Ortaköy district and its ophiolite at the western edge of the Middle Anatolian Massif, Turkey. *J. Afr. Earth Sci.* 18 (2), 163–174.
- Köksal, S., Göncüoğlu, M.C., 1997. Geology of the İdiş Dağı—Avanos area (Nevşehir—Central Anatolia). *Bull. Miner. Res. Explor.* 119, 41–58.
- Köksal, S., Romer, R.L., Göncüoğlu, M.C., Toksoy-Köksal, F., 2004. Timing of post-collisional H-type to A-type granitic magmatism: U–Pb titanite ages from the Alpine central Anatolian granitoids (Turkey). *Int. J. Earth Sci.* 93, 974–989.
- Köksal, S., Möller, A., Göncüoğlu, M., Frei, D., Gerdes, A., 2012. Crustal homogenization revealed by U–Pb zircon ages and Hf isotope evidence from the Late Cretaceous granitoids of the Ağaören intrusive suite (Central Anatolia/Turkey). *Contrib. Mineral. Petrol.* 163 (4), 725–743.
- Kröner, A., Şengör, A.M.C., 1990. Archean and Proterozoic ancestry in late Precambrian to early Paleozoic crustal elements of southern Turkey as revealed by single-zircon dating. *Geology* 18 (12), 1186–1190.
- Lefebvre, C., Barnhoorn, A., van Hinsbergen, D.J.J., Kaymakci, N., Vissers, R.L.M., 2011. Late Cretaceous extensional denudation along a marble detachment fault zone in the Kırşehir massif near Kaman, Central Turkey. *J. Struct. Geol.* 33 (8), 1220–1236.
- Lefebvre, C., Peters, K.M., Wehrens, P.C., Brouwer, F.M., van Hinsbergen, D.J.J., Kaymakci, N., Vissers, R.L.M., van Roermund, H.L.M., Advokaat, E.L., Hendriks, B.H.W., Corfu, F. P-T-t evolution and extensional exhumation history of a high-temperature complex (Hirkadağ Block, Central Anatolia). *Lithos*, submitted for publication.
- McFadden, P.L., McElhinny, L.W., 1988. The combined analysis of remagnetization circles and direct observations in palaeomagnetism. *Earth Planet. Sci. Lett.* 87, 161–172.
- Meijers, M.J.M., Kaymakci, N., van Hinsbergen, D.J.J., Langereis, C.G., Stephenson, R.A., Hippolyte, J.C., 2010. Late Cretaceous to Paleocene oroclinal bending in the central Pontides (Turkey). *Tectonics* 29, TC4016 <http://dx.doi.org/10.1029/2009TC002620>.
- Merrill, R.T., McFadden, P.L., 2003. The geomagnetic axial dipole field assumption. *Phys. Earth Planet. Inter.* 139 (3–4), 171–185.
- Moix, P., Beccalotto, L., Kozur, H.W., Hochard, C., Rosselet, F., Stampfli, G.M., 2008. A new classification of the Turkish terranes and sutures and its implications for the Paleotectonic history of the region. *Tectonophysics* 451 (1–4), 7–39.
- Okay, A.I., 1989. Tectonic units and sutures in the Pontides, northern Turkey. In: Şengör, A.M.C. (Ed.), *Tectonic evolution of the Tethyan region*. Kluwer Academic Publications, Dordrecht, pp. 109–115.
- Oktaç, F.Y., 1981. Stratigraphy and geological evolution of the sedimentary cover of the central Anatolian Massif in the Kaman-Kırşehir region. Turkish Geological Society, 35th Scientific and Technical Assembly, Symposium on the Geology of central Anatolia.
- Oktaç, F.Y., 1982. Ulukışla ve çevresinin stratigrafisi ve jeolojik evrimi. *Türk. Jeol. Kurumu Bül.* 25, 15–25.
- Piper, J.D.A., Gürsoy, H., Tatar, O., 2002. Palaeomagnetism and magnetic properties of the Cappadocian ignimbrite succession, central Turkey and Neogene tectonics of the Anatolian collage. *J. Volcanol. Geotherm. Res.* 117 (3–4), 237–262.
- Platzman, E.S., Tapirdamaz, C., Sanver, M., 1998. Neogene anticlockwise rotation of central Anatolia (Turkey): preliminary palaeomagnetic and geochronological results. *Tectonophysics* 299, 175–189.
- Poisson, A., Guezou, J.C., 1996. Tectonic setting and evolution of the sivas basin, Central anatolia, Turkey. *Int. J. Geol. Rev.* 38, 838–853.
- Sanver, M., Ponat, E., 1981. Kırşehir ve dolaylarına ilişkin paleomanyetik bulgular, Kırşehir Masifinin rotasyonu. *İstanbul Yerbilimleri* 2, 231–238.
- Seymen, I., 1981. Stratigraphy and metamorphism of the Kırşehir Massif around Kaman (Kırşehir—Turkey). *Bull. Geol. Soc. Turkish.* 24, 7–14.
- Seymen, I., 1983. Tectonic features of Kaman Group in comparison with those of its neighbouring formations around Tamadağ (Kaman-Kırşehir). *Bull. Geol. Soc. Turkish.* 26, 89–98.
- Seymen, I., 2000. Geology of the Kırşehir Massif between the Savcılıbeyit (Kaman) and Yeşilli (Kırşehir) villages. In: Proceedings of the Congress of Geosciences and Mining for the 75th anniversary of the Turkish Republic. Book 1, MTA Ankara, pp. 67–91 (in Turkish with English abstract).
- Şengör, A.M.C., Yılmaz, Y., 1981. Tethyan evolution of Turkey: a plate tectonic approach. *Tectonophysics* 75, 181–241.
- Tatar, O., Piper, J.D.A., Gürsoy, H., Temiz, H., 1996. Regional significance of neotectonic counterclockwise rotation in Central Turkey. *Int. Geol. Rev.* 38, 692–700.
- Tauxe, L., Kent, D.V., 2004. A simplified statistical model for the geomagnetic field and the detection of shallow bias in paleomagnetic inclinations: was the ancient magnetic field dipolar?. In: Channell, J.E.T., Kent, D.V., Lowrie, W., Meert, J.G. (Eds.), *Timescales of the Paleomagnetic Field*, vol. 145. AGU Geophysical Monograph, Washington, pp. 101–115.
- Tolluoğlu, A.Ü., Erkan, Y., 1989. Regional progressive metamorphism in the Central Anatolian Crystalline Basement, NW Kırşehir Massif, Turkey. *METU J. Pure Appl. Sci.* 22 (3), 19–41.
- Torsvik, T.H., Muller, R.D., Van der Voo, R., Steinberger, B., Gaina, C., 2008. Global plate motion frames: toward a unified model. *Rev. Geophys.* 46 (3).
- Türel, T.K., 1991. Geology, petrography and geochemistry of Ekecikdağ plutonic rocks (Aksaray region—Central Anatolia). Ph.D. Thesis. Middle Eastern Technical University (METU), Ankara, p. 194.
- Whitney, D.L., Dilek, Y., 1997. Core complex development in central Anatolia, Turkey. *Geology* 25 (11), 1023–1026.
- Whitney, D.L., Teyssier, C., Dilek, Y., Fayon, A.K., 2001. Metamorphism of the Central Anatolian Crystalline Complex, Turkey: influence of orogen-normal collision vs. wrench-dominated tectonics on P-T-t paths. *J. Metamorphic Geol.* 19 (4), 411–432.
- Whitney, D.L., Teyssier, C., Fayon, A.K., Hamilton, M.A., Heizler, M., 2003. Tectonic controls on metamorphism, partial melting, and intrusion: timing and duration of regional metamorphism and magmatism in the Niğde Massif, Turkey. *Tectonophysics* 376 (1–2), 37–60.
- Whitney, D.L., Hamilton, M.A., 2004. Timing of high-grade metamorphism in central Turkey and the assembly of Anatolia. *J. Geol. Soc. London* 161, 823–828.
- Whitney, D.L., Teyssier, C., Heizler, M.T., 2007. Gneiss domes, metamorphic core complexes, and wrench zones: Thermal and structural evolution of the Niğde Massif, central Anatolia. *Tectonics* 26 (5).
- Yalınız, K.M., Göncüoğlu, M.C., 1998. General geological characteristics and distribution of the Central anatolian Ophiolites. *Yerbilimleri* 20, 19–30.
- Yalınız, M.K., Göncüoğlu, M.C., Ozkan-Altiner, S., 2000. Formation and emplacement ages of the SSZ-type Neotethyan ophiolites in Central Anatolia, Turkey: palaeotectonic implications. *Geol. J.* 35 (2), 53–68.
- Zijderveld, J.D.A., 1967. A.C. demagnetization of rocks: analysis of results. In: Collinson, D.W., Creer, K.M., Runcorn, S.K. (Eds.), *Methods in Palaeomagnetism*. Elsevier, Amsterdam, New York, pp. 254–286.